



Accurate Blood Pressure Measurement Using Smartphone's Built-in Accelerometer

LEI WANG, Soochow University, China

XINGWEI WANG, Soochow University, China

YU ZHANG, Macquarie University, Australia

XIAOLEI MA, Soochow University, China

HAIPENG DAI, Nanjing University , China

YONG ZHANG, Shenzhen Institutes of Advanced Technology, CAS, China

ZHIJUN LI, Soochow University, China

TAO GU, Macquarie University , Australia

Efficient blood pressure (BP) monitoring in everyday contexts stands as a substantial public health challenge that has garnered considerable attention from both industry and academia. Commercial mobile phones have emerged as a promising tool for BP measurement, benefitting from their widespread popularity, portability, and ease of use. Most mobile phone-based systems leverage a combination of the built-in camera and LED to capture photoplethysmography (PPG) signals, which can be used to infer BP by analyzing the blood flow characteristics. However, due to low Signal-to-Noise (SNR), various factors such as finger motion, improper finger placement, skin tattoos, or fluctuations in environmental lighting can distort the PPG signal. These distortions consequentially affect the performance of BP estimation. In this paper, we introduce a novel sensing system that utilizes the built-in accelerometer of a mobile phone to capture seismocardiography (SCG) signals, enabling accurate BP measurement. Our system surpasses previous mobile phone-based BP measurement systems, offering advantages such as high SNR, ease of use, and power efficiency. We propose a triple-stage noise reduction scheme, integrating improved complete ensemble empirical mode decomposition with adaptive noise (ICEEMDAN), recursive least squares (RLS) adaptive filter, and soft-thresholding, to effectively reconstruct high-quality heartbeat waveforms from initially contaminated raw SCG signals. Moreover, we introduce a data augmentation technique encompassing normalization coupled with *temporal-sliding*, effectively augmenting the diversity of the training sample set. To enable battery efficiency on smartphone, we propose a resource-efficient deep learning model that incorporates resource-efficient convolution, shortcut connections, and Huber loss. We conduct extensive experiments with 70 volunteers, comprising 35 healthy individuals and 35 individuals diagnosed with hypertension, under a user-independent setting. The excellent performance of our system demonstrates its capacity for robust and accurate daily BP measurement.

CCS Concepts: • Human-centered computing → Ubiquitous and mobile computing systems and tools.

Additional Key Words and Phrases: Seismocardiography, Blood Pressure.

Authors' Contact Information: Lei Wang, Soochow University, China, Email:wanglei@suda.edu.cn; Xingwei Wang, Soochow University, China, xw.wang@siat.ac.cn; Yu Zhang, Macquarie University, Australia, y.zhang@mq.edu.au; Xiaolei Ma, Soochow University, China; Haipeng Dai, Nanjing University , China, Email:haipengdai@nju.edu.cn; Yong Zhang, Shenzhen Institutes of Advanced Technology, CAS, China, zhangyong@siat.ac.cn; Zhijun Li, Soochow University, China, zjli@suda.edu.cn; Tao Gu, Macquarie University , Australia, Email: tao.gu@mq.edu.au.

Permission to make digital or hard copies of all or part of this work for personal or classroom use is granted without fee provided that copies are not made or distributed for profit or commercial advantage and that copies bear this notice and the full citation on the first page. Copyrights for components of this work owned by others than the author(s) must be honored. Abstracting with credit is permitted. To copy otherwise, or republish, to post on servers or to redistribute to lists, requires prior specific permission and/or a fee. Request permissions from permissions@acm.org.

© 2024 Copyright held by the owner/author(s). Publication rights licensed to ACM.

ACM 2474-9567/2024/5-ART57

<https://doi.org/10.1145/3659599>

ACM Reference Format:

Lei Wang, Xingwei Wang, Yu Zhang, Xiaolei Ma, Haipeng Dai, Yong Zhang, Zhijun Li, and Tao Gu. 2024. Accurate Blood Pressure Measurement Using Smartphone's Built-in Accelerometer. *Proc. ACM Interact. Mob. Wearable Ubiquitous Technol.* 8, 2, Article 57 (June 2024), 28 pages. <https://doi.org/10.1145/3659599>

1 INTRODUCTION

Hypertension, also known as high blood pressure, is a medical condition characterized by the elevated force exerted by blood against the walls of the arteries as it circulates throughout the body [23]. The World Health Organization reports that an estimated 1.28 billion adults aged 30 to 79 globally suffer from hypertension [1]. This condition is responsible for 7.5 million deaths annually, constituting 12.8% of all global deaths. Notably, hypertension is often asymptomatic, significantly hindering early detection. Consequently, monitoring BP in our daily lives is a substantial public health challenge that has garnered considerable attention from both the industrial and academic sectors.

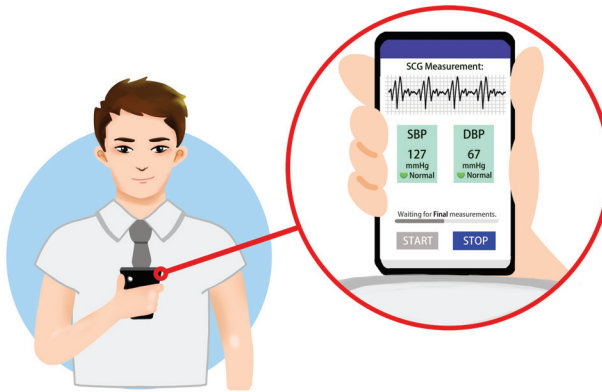


Fig. 1. Typical application scenario of our system for BP measurement.

BP measurement in the consumer market is commonly done through the automatic oscillometric method[55, 61]. However, limitations in daily monitoring arise from the fact that users usually use arm cuff-based measurements. Arm-cuff-based devices are generally inconvenient to operate, especially for elderly people who may feel discomfort or tightness during measurements. Some hypertensive patients require multiple blood pressure measurements, i.e., 20 times in a day [52], to mitigate the risk of stroke, but measurements in a day may cause tissue hypoxia risk [9, 28].

Many efforts in the academic community have emerged to measure BP, focusing primarily on two main schemes: contact-based and contact-free. For contact-based BP measurement, PPG systems [27, 68] have become prevalent due to the attributes of the pulse wave associated with BP, including characteristics such as peak value, rising time, and the first inflection point [7]. In the pursuit of this objective, various BP measurement systems have successfully demonstrated the utility of pulse-related physiological signals, which are typically derived from specialized devices [10, 12, 59], such as wristwatches or finger cuffs. Despite the promise of these methodologies, certain limitations persist. First, these systems demand that the user remains completely stationary to capture data with an extremely low signal-to-noise ratio (SNR), a requirement often challenging to meet in real-life scenarios. Furthermore, the requirement for users to wear these devices can lead to discomfort and inconvenience, which presents a significant challenge to the broader implementation and acceptance of these technologies. The contact-free schemes leverage

mainly on wireless signals, e.g., millimeter wave [37, 58] and continuous wave [8], to detect subtle changes in the skin resulting from pulse activity, thereby effectively deriving BP measurements. However, most of them involve costly, dedicated instruments, rendering them far from practical use. Furthermore, these stationary devices operate only when users are within a specific area, hindering the possibility of location-independent daily BP monitoring.

Recently, commercial mobile phones have emerged as an ideal alternative for BP measurement, owing to widespread popularity, portability. Most mobile phone-based systems utilize a combination of built-in cameras and LEDs to capture PPG signals, which can be leveraged to infer BP by analyzing the blood flow characteristics [6, 20, 23, 25, 47]. However, the pulsatile component in mobile phone's camera signals accounts for just 1% of the total intensity, resulting in a low SNR for the PPG signal. Various factors such as finger motion, improper finger placement, skin tattoos, or changes in environmental lighting can distort the PPG signal, thereby affecting subsequent BP estimation [23]. Mitigating these adverse effects can be partially achieved through the integration of signals from other built-in sensors, such as microphone [40] or accelerometer [64]. However, manual intervention is needed to synchronize these multiple sensors prior to each measurement, which is inconvenient, particularly for the elderly. In this paper, we introduce a novel sensing system that utilizes the built-in accelerometer of a mobile phone to capture SCG signals, enabling accurate BP measurement. The critical insight lies in the fact that SCG signals are highly sensitive to dynamic changes, enabling them to effectively capture the various phases of the cardiac cycle, including both systolic and diastolic states. This characteristic forms the basis for accurate BP. Our system surpasses previous mobile phone-based BP measurement systems, offering advantages such as high SNR, ease of use, and power efficiency. We have created a promising scenario for the everyday monitoring of BP, where a user can simply press the mobile phone against his/her chest anytime and anywhere, as illustrated in Fig. 1, and the system will quickly measure BP and record the data in the user's health profile. This approach will facilitate early detection and screening for cardiovascular diseases.

Despite promising, several challenges need to be addressed before enabling the functional system. The first challenge is to reconstruct high-quality heartbeat waveforms from raw SCG signals. During the signal acquisition process, the acceleration data includes the heartbeat signal as well as noise from the system, respiration, and motion artifacts, all of which may distort the waveform characteristics. To address this challenge, we propose a triple-stage noise reduction scheme: i) reduce the effects of movement artifacts through the ICEEMDAN method, ii) further filter out the effect of residual movement noise to clarify the heartbeat pattern using the RLS adaptive filter, and iii) remove the residual minor spike noise (e.g., system noise) using the soft-thresholding method. The second challenge is the lack of training samples, which may be costly to collect manually. Instead, we collect a limited amount of raw data only and use two-step data augmentation techniques to enhance its diversity. We first normalize the data to eliminate the influence of gravity and pressure based on the observation that these factors only affect the magnitude or range of acceleration changes, not the pattern of change. We then implement the *temporal-sliding* approach to increase the temporal sampling, which involves multiplying the original data points with a sliding window of fixed amplitude. This approach is motivated by our observation that different sample starting points can significantly impact the pattern of the data. The third challenge is to develop a lightweight yet high-precision BP measurement model, capable of functioning on resource-constrained commercial smartphones. State-of-the-art deep learning models with complex multiple-layer model structures, such as ResNet50, result in considerable *resource overhead*. When deployed to smartphones, they can lead to substantial memory footprints and increased latency, and may easily yield *overfitting* with an accuracy drop. A possible solution is to involve employing models with fewer layers, such as LeNet with only two convolutional layers. However, it may result in *underfitting* and compromised accuracy due to the restricted number of layers. To address these challenges, we introduce a novel, resource-efficient BP model that facilitates lightweight model deployment while maintaining high accuracy and robustness on smartphones. Specially, we employ a suite of techniques to substantially reduce resource overhead and enhance the overall performance of the BP model, including resource-efficient convolution, shortcut connections, and Huber loss.

In summary, this paper makes the following contributions.

- To the best of our knowledge, we are the first to create a highly accurate BP measurement system solely relying on the built-in accelerometer of a mobile phone. Our system is superior to previous mobile phone-based BP methods, providing advancements such as high SNR, ease of use, and energy efficiency. We've established a promising scenario for daily BP monitoring that requires only pressing a mobile phone against the chest anytime and anywhere. The system swiftly measures BP, stores the data in the user's health profile, and aids in the early detection and screening of cardiovascular diseases.
- We propose a triple-stage noise reduction scheme, consisting of ICEEMDAN, RLS adaptive filter, and soft-thresholding, to effectively reconstruct high-quality heartbeat waveforms from contaminated raw SCG signals. Moreover, we introduce a data augmentation technique, encompassing normalization coupled with *temporal-sliding*, effectively augmenting the diversity of the training sample set. To enable battery efficiency on smartphone, we propose a resource-efficient deep learning model that incorporates resource-efficient convolution, shortcut connections, and Huber loss.
- We successfully implement our system on Android smartphones and conduct extensive experiments with 70 volunteers—35 healthy individuals and 35 individuals diagnosed with hypertension—in a user-independent setting. The results reveal that the mean error (ME) and standard deviation (SD) for diastolic blood pressure (DBP) are 0.93 mmHg and 5.27 mmHg, respectively. For systolic blood pressure (SBP), the ME and SD are 1.81 mmHg and 5.91 mmHg, respectively. The results demonstrate that our system is capable of robust and accurate daily BP measurement.

2 RELATED WORK

Contact-based BP measurement: The mercury sphygmomanometer method is currently the gold standard for contact-based BP measurement [38, 54]. This technique involves a BP cuff with an attached airbag, which is progressively inflated on the upper arm to halt arterial blood flow. Gradual deflation of the airbag, followed by the placement of a stethoscope on the brachial artery, allows medical practitioners to measure both systolic and diastolic pressures. However, due to its complexity and the requirement for trained medical personnel, this method is impractical for everyday use. Another contact-based BP measurement technique available in the consumer market is the automatic oscillometric method [55, 61]. This approach involves attaching a cuff to the arm, injecting gas, and then methodically releasing the gas while monitoring arterial pressure to measure BP. However, its application in daily monitoring is limited as users typically rely on arm cuff-based measurements. PPG systems [27, 68] have gained popularity due to their ability to analyze pulse wave attributes associated with BP [7]. A lot of efforts have been devoted to exploring the feasibility of estimating BP based on pulse-related physiological signals, which are captured using specialized devices [10, 12, 59], e.g., wrist-worn devices, finger cuffs. Cao *et al.* [9] demonstrate that a single PPG sensor embedded in wrist-worn devices can effectively produce arterial blood pressure measurements. BioWatch [62] employs both ECG and PPG to measure the proximal and distal timing of blood flow for BP monitoring, respectively. Similarly, Huynh *et al.* [34] introduce a wrist-worn device that uses bioimpedance and PPG to determine pulse transit time for BP measurement. Yousefian *et al.* [69] propose combining PPG and ballistocardiogram (BCG) signals acquired at the wrist for blood pressure measurement. Chang *et al.* [13] propose that the SCG signals, captured by dedicated accelerometers embedded in a chest strap, can also be used for inferring blood pressure. However, these systems require the user to keep completely stationary while collecting samples, which is challenging to fulfill in practical settings. Moreover, the experience of wearing these devices can result in discomfort and inconvenience for the users. Therefore, it is challenging to enable broader implementation and acceptance of these technologies. In comparison, our system is deployed on the commodity smartphone. The user simply needs to press the phone against their chest to immediately acquire blood pressure readings, making it

highly convenient and user-friendly for adoption. Additionally, we have implemented a triple-stage noise reduction scheme to effectively mitigate the negative effects of movement artifacts.

Contact-free BP measurement: Contact-free methods predominantly rely on variations in wireless signals, such as millimeter wave [37, 41, 42, 45, 56, 58, 66] and continuous wave [8, 73], and ultra-wideband signals [43] to detect subtle skin changes caused by pulse activity, effectively deriving BP measurements. For example, Kawasaki *et al.* use millimeter-wave sensors to extract time-domain features for BP estimation [41]. Similarly, Shi *et al.* investigate the estimation of systolic BP by leveraging the reflective properties of millimeter waves [57]. Kim [43] proposes a radio frequency-based system that collects and processes ultra-wideband signals to extract key features for BP measurement. Zhao *et al.* [73] develop a Doppler radar-based BP measurement system by processing continuous wave signals. However, most of these approaches require expensive, specialized equipment, making them impractical for widespread use. Additionally, these stationary devices only operate when users are within a specific area, limiting the potential for location-independent daily BP monitoring. In contrast, our system, deployed on smartphones, is not limited by the user's location.

Mobile phone based BP measurement: Commercial mobile phones have emerged as a promising modality for BP measurement due to their ubiquity and portability. Most mobile phone-based systems employ a combination of built-in cameras and LEDs to capture PPG signals, which can be used to infer BP by analyzing blood flow characteristics [6, 20, 23, 25, 47]. However, the pulsatile component of the camera signals in mobile phones is small, resulting in a low SNR for the PPG signal. Several factors, such as finger motion, incorrect finger positioning, skin tattoos, and fluctuations in environmental lighting, can adversely affect the PPG signal, affecting the subsequent BP estimation [23]. Combining PPG with other embedded modalities, including microphones [40] and accelerometers [64], may counteract the negative impact. However, the PPG based BP system faces two significant limitations. Firstly, each measurement necessitates manual synchronization of multiple modalities, which is inconvenient. Secondly, the frequent activation of LED lights not only accelerates battery depletion but may also cause discomfort to users, especially in low-light environments. Other mobile phone-based systems rely on fingertip photoplethysmometry to estimate BP [11, 65]. As a user presses the finger against the smartphone, the external pressure on the underlying artery gradually rises, while the phone concurrently measures the applied pressure and blood volume oscillations. The smartphone provides visual feedback to guide the user in applying the correct pressure and instantly calculates the BP. However, these methods require either adding extra hardware to the smartphone, such as PPG and force sensors, or using the smartphone in conjunction with other hardware, like a plastic clip, both may be impractical for daily use. In contrast to previous systems, we present a novel sensing system that leverages the built-in accelerometer of a smartphone to capture SCG signals, enabling accurate BP measurement. This approach offers several advantages, such as high SNR, ease of use, and power efficiency.

3 FEASIBILITY STUDY

Seismocardiography (SCG) is a non-invasive method that gathers information by tracking the vibrations of the chest collected by accelerometers. SCG signals reflect the heart's mechanical activities by capturing the timing and duration of both the systolic (the contraction of the heart muscle) and diastolic (the refilling of the heart) motions. As shown in Fig. 2, there are generally seven stages in a whole cardiac cycle [19, 21, 24, 35]. The first stage is atrial contraction (ATC). During this stage, the atrial muscles contract, pushing blood from the atria to the ventricles. The second stage is mitral valve closure (MC). This stage signifies a swift surge in intraventricular pressure, causing the mitral valve to shut and, thus, preventing the backflow of blood into the atria. The third stage is aortic valve opening (AO). When ventricular pressure exceeds that in the aorta, the aortic valve opens, allowing blood to flow from the ventricles into the aorta and then throughout the body. The fourth stage is maximal blood acceleration in the aorta (MA). In this stage, the heart muscle undergoes contraction, instigating a swift ejection of blood from the left ventricle into the aorta. The fifth stage is aortic valve closure (AC). This stage signifies the cessation of the

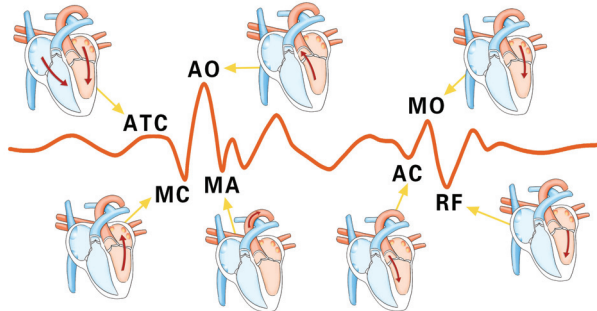


Fig. 2. Stages of full heartbeat motion within a cardiac cycle.

heart's systolic stage and the initiation of the diastolic phase. The next stage is mitral valve opening (MO). This triggers the flow of blood from the left atrium into the left ventricle, indicating the commencement of the filling phase in the cardiac cycle. The last stage is referred to rapid filling of the left ventricle (RF). In this stage, a rapid influx of blood from the atrium into the ventricle is facilitated due to the higher BP in the left atrium compared to the left ventricle.

The events of the cardiac cycle corresponding to the positive or negative peaks can be discernibly pinpointed through SCG signals procured by standalone accelerometers, such as SCA610-C21H1 A [53] and LIS3DSH [13], as depicted in Fig. 2. Given that most mobile devices come standard with accelerometers, the potential to measure SCG signals by simply positioning the phone against the chest is promising [44, 49, 60]. As depicted in Fig. 3, we vertically press the phone against the chest and hold our breath for 5 seconds. In examining the measurements from the accelerometer's X, Y, and Z axes, we find that the Y-axis waveform displays more pronounced periodicity compared to the other axes. This characteristic is likely due to the heart's primary activity occurring along the Y-axis. In comparison, the components of heart motion in the X and Z axes are less significant, making the effects of noise more noticeable. Consequently, since the composite amplitude $\sqrt{X^2 + Y^2 + Z^2}$ combines the outcomes from these three directions, it naturally has a weaker performance in capturing heart movement compared to the results obtained in the Y-axis. Our data from Y-axis reveal a signal with an SD of 0.04 m s^{-2} during the cardiac cycle, in contrast to an SD of 0.01 m s^{-2} in a fully static state. Consequently, this significant SNR is more than adequate to capture the various events within each cardiac cycle. Therefore, we utilize the Y-axis readings of the accelerometer for measuring blood pressure.

The above results adequately demonstrate that the accelerometer in a smartphone is capable of capturing cardiac activity for further analysis. Besides, since previous research has employed a range of custom-made wearable devices to investigate the pronounced correlation between certain waveform characteristics, such as wave amplitude and time intervals, in various signals (including PPG [9], Ballistocardiography (BCG) [69], and SCG [13]) and BP. The above analysis implies the significant feasibility to predict BP using waveform attributes of SCG signals collected from built-in accelerometers in smartphones.

4 TRIPLE-STAGE NOISE REDUCTION

In this section, our concentration is directed toward the extraction of meaningful cardiac patterns from the SCG measurements, which are encumbered by various sources of noise, inclusive of system noise, respiratory activity, and movement artifacts (e.g., physiologic tremor and sudden unintentional flutter).

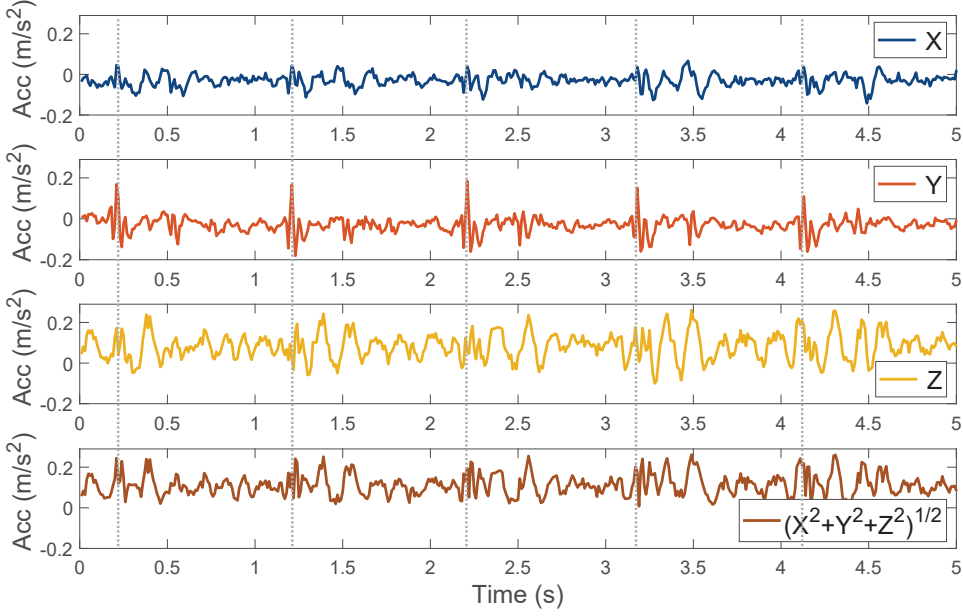


Fig. 3. SCG signals captured from the X, Y, and Z axes by the built-in accelerometer of a mobile phone.

4.1 ICEEMDAN-based Heartbeat Extraction

The first step is to extract the heartbeat pattern from the contaminated SCG measurements, as shown in Fig. 4(a). In this scenario, we instruct a subject to sit with a phone in hand, pressed against chest, and to suddenly perform a hand trembling operation between 2nd and 3rd seconds. Since the mixed SCG signal is nonlinear and unstable signals, the basic insight is to decompose the mixed signal into different components with various motion patterns. The commonly used method involves using wavelet transforms, e.g., discrete wavelet transform (DWT) [31] and stationary wavelet transform (SWT) [51], to decompose the signal into components within different frequency ranges by selecting specific wavelet functions. However, the decomposition performance of wavelets relies heavily on the basis wavelet function, which is challenging to reflect the intrinsic characteristics of SCG signals from various subjects.

In our system, we utilize empirical mode decomposition (EMD) [33]—an adaptive technique well-suited for non-stationary and nonlinear time-varying sequence analysis. Instead of a specified basis function in wavelet-based method, EMD decomposes the temporal sequences into a succession of independent time-frequency components, which is called intrinsic mode function (IMF), aiding in the extraction of heartbeat patterns. This is mainly due to that the IMF components are instantaneous frequency components, representing local characteristics of the original signal at various time scales, making EMD exceptionally suitable for the analysis of non-linear and non-stationary data.

However, this introduces a potential challenge in EMD, referred to as “mode mixing”. Here, disparate scale oscillations can occur within the same mode, or similarly scaled oscillations may manifest across different modes, complicating the extraction of heartbeat patterns. Building upon EMD, the Complete Ensemble empirical mode decomposition with adaptive noise (CEEMDAN) technique [63] has been proposed as a resolution to the mode-mixing problem, achieved through the integration of adaptive white noise. Nonetheless, this method grapples with two significant issues: residual noise within the modes and the emergence of spurious modes during the

decomposition process. An advancement of EMD-based techniques, known as ICEEMDAN [18], has proven effective in addressing these aforementioned challenges. As such, we employ ICEEMDAN for the extraction of heartbeat patterns in our system.

By employing the ICEEMDAN decomposition method, as detailed in [18], we decompose the targeted SCG signal into five distinct IMFs, as shown in Fig. 4(b). We note that the heartbeat signal is distinctly prominent in IMF1, displaying marked periodic features. Consequently, we exclusively utilize IMF1 for the reconstruction of the heartbeat signal. The result demonstrates that ICEEMDAN effectively eliminates the majority of noise, specifically noise resulting from abrupt fluctuations occurring between 2.5 and 3.2 seconds. Nevertheless, due to the pseudo-periodicity of heartbeat and instability of noise, ICEEMDAN is unable to completely eradicate all noise, which necessitates further filtering procedures.

4.2 RLS-based Filtering

Although ICEEMDAN significantly reduces the influence of hand trembling, it does not entirely succeed in eradicating them, resulting in the presence of residual noise. Consequently, this results in a segment of the signal devoid of a clearly distinguishable pattern. In this subsection, we focus on further filtering out the effect of residual movement artifacts.

Before employing the RLS filter, it is requisite to have a reference signal that embodies the ideal output or anticipated state of the system. In contrast to the noisy period, the SCG morphology consistently displays periodic features and a similar pattern during other silent periods. Thus, we can designate the signal within the quiescent period as the reference signal. Now, how can we accurately identify and extract segments with similar patterns? Our fundamental insight is that similar segments exhibit a high correlation, while dissimilar ones yield a lower correlation. Upon this concept, our approach is outlined as follows: First, we divide the ICEEMDAN output into K segments. To ensure that each segment fully captures the holistic attributes of the SCG morphology, the segment length is stipulated to lie within one to two periods. Then, for any two segments, we derive the similarity by calculating the Pearson correlation coefficient [17]. Following this, we construct a $K \times K$ similarity matrix. Segments with similarity exceeding an empirical threshold of 0.7 are considered as candidates. Finally, the segment appearing most frequently in this candidate set is identified as the temporal reference, exemplified by the segment from 8 to 9 seconds in IMF1, as depicted in Fig. 4(b). Then we further filter IMF1 according to the standard process of the RLS filter [16] to remove the residual effects of movement artifacts. Fig. 4(c) illustrates a substantial reduction in movement noise, resulting in a more discernible heartbeat pattern in contrast with the results obtained solely using ICEEMDAN, as depicted in Fig. 4(b).

4.3 Residual Noise Removal

While the previous techniques prove highly effective in eliminating most of the movement noise, a small amount of residual minor spike noise persists. In this paper, we introduce a lightweight denoising algorithm, referred to as soft-thresholding [5, 22, 39], designed to further enhance the extraction of clear cardiac vibrations. The denoising scheme is implemented through the following two steps. First, the algorithm computes the empirical global threshold, as represented in [39], which can be expressed as follows:

$$\varrho = \delta_0 \sqrt{2 \ln(N)}, \quad (1)$$

where N represents the length of the data, and δ_0 denotes the noise level, defined as follows:

$$\delta_0 = \frac{\text{median}(|S_n - \text{median}(S_n)|)}{0.6475}, \quad (2)$$

where S_n represents the value in the purified SCG sequence following the previous RLS filter. Next, we apply the soft-thresholding technique to each element of the sequence, utilizing the chosen global threshold as follows:

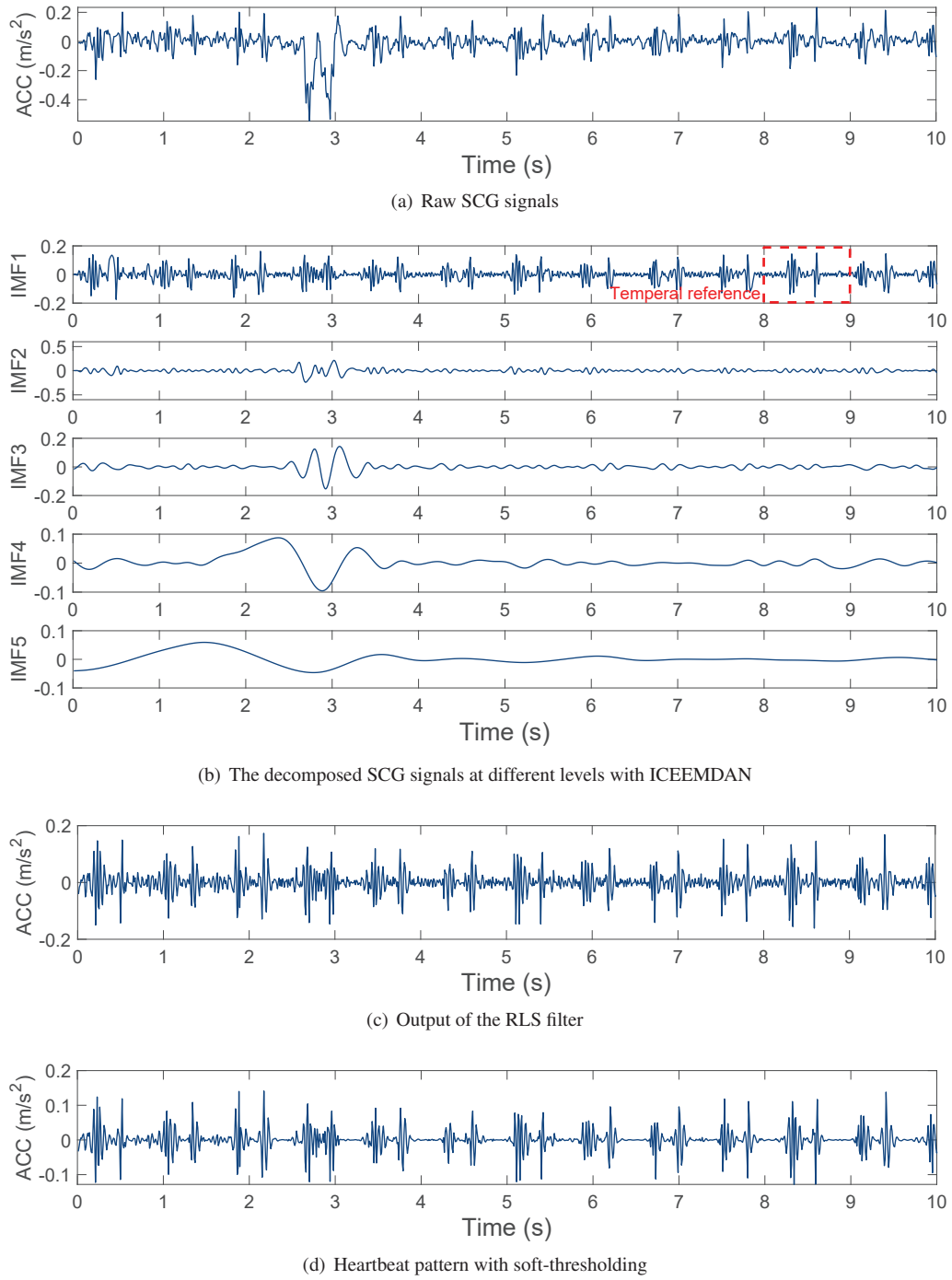


Fig. 4. Triple-stage noise reduction for cardiac pattern extraction.

$$v(n) = \text{sign}(S_n) \cdot (|S_n| - \varrho)_+. \quad (3)$$

Here, v_+ is defined as v when $v \geq 0$, and is 0 otherwise. It is important to note that this step assesses each element based on its absolute value relative to the threshold. Elements that exceed the threshold ϱ are retained by subtracting the threshold while preserving the original sign. This procedure effectively filters out low-amplitude noise components and retains the primary characteristics of the signal. Consequently, the soft-thresholding technique further refines the SCG signals, producing a more pronounced heartbeat pattern, as depicted in Fig. 4(d).

5 ENHANCEMENT OF DATA DIVERSITY

When the mobile phone's accelerometer captures the SCG signal, our system will use its waveform characteristics to infer BP with deep learning model. However, the accuracy of this recovery may be affected by a lack of diverse training samples. In this subsection, we introduce two steps to ensure the data covers most potential situations.

The first step involves minimizing the variations in SCG amplitude to ensure that heartbeats collected under diverse conditions exhibit consistent and comparable amplitudes. The amplitude of SCG signals depends on the angle between the mobile phone's y-axis and the user's chest, the position of the mobile phone, and the pressure applied to it. Since our system allows users to collect SCG signals in slightly different ways, we need to eliminate these influences. As a result, the amplitudes of the SCG signals collected under various conditions differ from one another. To validate this, we recruit a volunteer to collect 100 samples of SCG signals. Note that each sample contained 10 seconds of data, corresponding to 1000 points at a sampling rate of 100 Hz. In each sample collection, the volunteer was instructed to hold the smartphone against his chest at varying intensities, positions, and angles. Note that “different intensities” here refers to the varying levels of pressure applied by the phone against the chest. “Different positions” means areas within a 5 cm range to the left, right, and below the reference point. “Different angles” refers to the phone being tilted up or down by no more than 45°. We observe that despite the consistency of heartbeat waveform patterns across different situations, the range of amplitude significantly varies, influenced by the angle, position, and pressure of the mobile phone. To reduce variations in SCG signals, we used the Min-Max method to normalize SCG measurements to the same range, i.e., 0 ~ 1.

The second step involves enriching the training samples by incorporating various starting points. Since different starting points yield a variety of waveform patterns for a given length of sampled data, the limited number of samples reflects a lack of variation in the data, thereby making the BP estimation challenging. To enhance data diversity, one intuitive solution is to increase the number of random samples collected multiple times. However, this approach is both labor-intensive and time-consuming. In our system, we introduce a *temporal-sliding* scheme to enhance the diversity of the training data. This method involves calculating the dot product between a sliding window of constant magnitude 1 and the collected SCG sequence. We utilize the result of each dot product as a new sample, thereby incorporating new samples that encompass all possible starting points within a heartbeat cycle. For example, when we collect 11 seconds of purified SCG data represented by the sequence $[S(1), S(2), \dots, S(1100)]$, we perform the dot product operation with a sliding window length of 1000 (10 seconds at a sampling rate of 100 Hz), we can get 100 sample sequences through the dot product operation: $[S(1), S(1), \dots, S(1000)]$, $[S(2), S(3), \dots, S(1001)]$, ..., $[S(100), S(101), \dots, S(1099)]$. Given that the typical cardiac cycle for most individuals ranges between 60 and 100 beats per minute, 100 consecutive sampling points are generally sufficient to cover the majority of potential starting point scenarios. By leveraging the low-cost augmentation method, we can avoid overfitting and improve the generalization performance of the system, thus further enhancing the capability of the system in BP estimation.

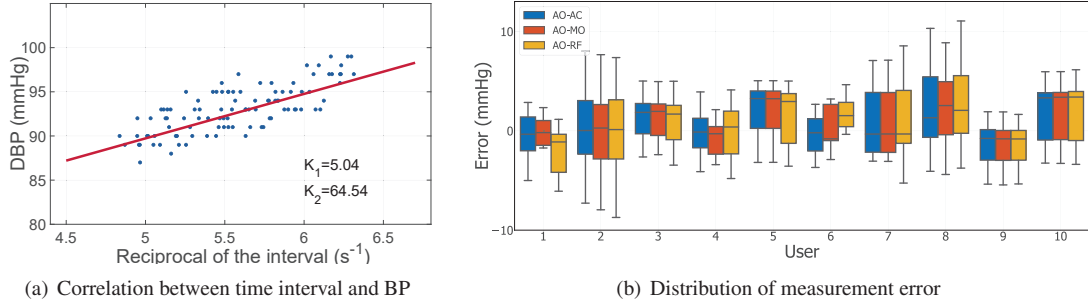


Fig. 5. Performance of the quantitative BP estimation model.

6 DEEP LEARNING BASED BP MEASUREMENT

6.1 Limitations of Possible BP Models

6.1.1 Linear Correlation-based BP Model. A reasonable method for measuring BP involves quantitatively assessing the relationship between BP and time intervals, a crucial feature of waveform. As we know, a complete heartbeat cycle includes two phases: systole and diastole. During the systolic phase, the aorta circulates blood throughout the body, reaching areas such as the fingertips and ears, while veins, during the diastolic phase, return blood from these same regions back to the heart. Therefore, the interval between different states of the systolic and diastolic phases is inversely related to the wave velocity. This implies that the time interval between varied states within the systolic and diastolic phases could be characterized as a variant of pulse transit time (PTT), which is employed as a basis for the quantitative estimation of BP. Thus, the relationship between BP and time interval can be mathematically expressed as follows [26]:

$$BP = \frac{K_1}{\Delta\tau} + K_2, \quad (4)$$

where K_1 and K_2 are subject-specific parameters, and $\Delta\tau$ indicates the time interval between different states in the cardiac cycle.

We carefully prove this assumption by delving into the following specific aspects: First, we recruited one volunteer to perform various activities (to increase the range in BP), including walking, and jogging, followed by remaining still for two minutes to measure their SCG and DBP. Subsequently, we collected 100 recordings of SCG signals from the subject, while concurrently recording their BP using an Omron J751 BP monitor [2]. It should be noted that one recording corresponds to a random heartbeat cycle captured within a collection period of 10 seconds. For each SCG reading, we calculated the reciprocals of the intervals between critical cardiac states (such as AO to AC, AO to MO, AO to RF). Due to space constraints, here we only demonstrate the relationship between the reciprocal of the AO to MO interval and blood pressure. As demonstrated in Fig. 5(a), a distinct linear correlation is observed between the reciprocal of the AO to MO interval and BP. Second, to further explore whether the intervals within the heartbeat cycle can be used to predict BP and be applicable to a wider range of users, we hired 10 subjects to collect 300 SCG samples and ground truth BP readings each. For each subject, we used 100 of the samples to train the subject-specific parameters (i.e., K_1, K_2) using the least square method for three different time intervals (i.e., AO-AC, AO-MO, AO-RF), and the remaining 200 samples were used to calculate the measurement error, which was determined by subtracting the reference DBP. Fig. 5(b) demonstrates that the BP measurement model based on a linear relationship exhibits acceptable performance for all subjects. Specifically, for all subjects, ME stays below 2.17 mmHg, and SD remains under 5.02 mmHg across all time intervals, both of which fall within the acceptable error range established by Association for the Advancement of Medical Instrumentation (AAMI).

Table 1. Performance comparison using different models on a commercial smartphone.

Model	Params (M)	FLOPs (G)	Latency (ms)	DBP Error (mmHg)	SBP Error (mmHg)	Memory (MB)
LeNet	0.23	0.05	20	2.08±9.23	-3.09 ± 10.80	51
ResNet50	15.96	11.09	1227	-0.99 ± 7.55	2.20 ± 8.11	187
Ours	0.28	0.21	44	0.93 ± 5.27	1.81 ± 5.91	56

Although we have already demonstrated that we can quantitatively estimate BP by capturing the time intervals of each cardiac stage in the heart cycle based on the linear correlation method, this method has two significant limitations. Firstly, as depicted in Figure 3, aside from the AO point, the amplitude of other points is generally weak, which makes them susceptible to submersion and challenging to locate. Secondly, the parameters K_1 and K_2 vary among the linear correlation models of different subjects. Consequently, estimating the parameters for different subjects requires the collection of a substantial number of samples, which is clearly inconvenient. Instead, we aim to establish a robust correlation between BP and SCG patterns that is applicable to a broad range of subjects, thus enabling high-precision BP prediction.

6.1.2 Existing Deep Learning Models. To bridge the correlation, our objective is to build an optimal deep learning model f^* to minimize the loss $L(\cdot)$ between the actual BP, i.e., Y , and the predicted BP, i.e., $\hat{Y} = f(X)$, where X denotes the purified SCG defined as $X = \{x_i\}_{i=1}^t$, and t denotes the SCG time steps. Hence, our BP prediction problem is formulated as follows.

$$f^* = \underset{f}{\operatorname{argmin}} L(Y, f(X)). \quad (5)$$

As aforementioned, we aim to deploy our system directly on commercial smartphones with accurate BP measurement. Beyond accuracy, another critical factor, multiple measurements, should be carefully considered. This is because BP measurement exhibits randomness, and averaging multiple measurements within the same period can effectively reduce this randomness [46] (as detailed in Fig. 22, we have experimentally verified that multiple measurements can effectively minimize measurement errors). Moreover, for hypertension patients, measuring BP at various times throughout the day can reduce the risk of stroke [52]. Multiple measurements inevitably lead to critical consumption of resources. However, the resources of smartphones are quite limited, hence, if we need to implement BP monitoring on smartphones, we urgently require an accurate and lightweight deep learning model.

The state-of-the-art deep learning models (e.g., ResNet50) inherently involve a large number of floating number operations (FLOPs) and millions of parameters in convolutional and fully-connected layers [14]. However, due to resource constraints on smartphones (e.g., limited computational resources and memory), deploying the state-of-arts can lead to critical *resource overhead*, resulting in massive memory footprint and high latency [72]. Besides, these existing models are usually designed with a large number of layers to enhance model accuracy, but such complex multiple-layer model structures may easily yield *overfitting* with accuracy drop when applied to sensing applications [70]. A straightforward solution leverages a simple model with a small number of layers, but it may result in *underfitting* with low accuracy due to the limited number of layers [50].

To quantify the performance of deploying the existing models on a smartphone (i.e., Samsung S10), we conduct a preliminary study and examine both pre-trained LeNet and ResNet50 based on our BP dataset with detailed specifications shown in Section 8.1. We also use the Leave-One-Out Cross-Validation (LOOCV) to evaluate the performance using different models, incorporating data from 70 users. The results in Table 1 reveal that the ResNet50 achieves a high model inference latency of 1227 ms on average and a large memory footprint of 187 MB on average caused by a large number of parameters and FLOPs. Such high latency may be practically limited for continual BP monitoring in real time. Although the LeNet achieves much lower latency and memory footprint (e.g.,

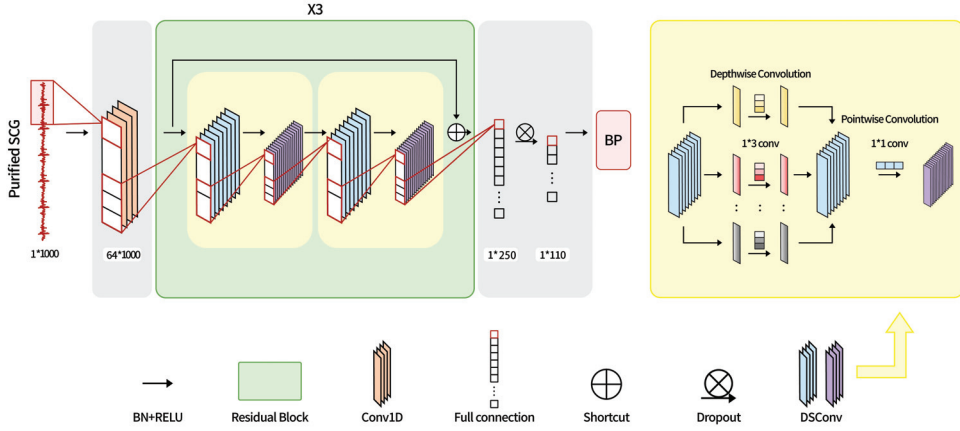


Fig. 6. Accurate and resource-efficient BP model structure.

20 ms and 51 MB on average), it results in a high mean error of BP prediction due to the limited model structure. Additionally, the model accuracy using ResNet50 is compromised by overfitting.

6.2 Accurate and Efficient BP Model Design

To address the challenges of resource overhead and low accuracy, we propose a new accurate and resource-efficient BP model that enables lightweight model deployment with high accuracy and robustness on smartphones. This capability is essentially achieved by the proposed resource-efficient model structure shown in Fig. 6. We also apply a set of techniques to significantly reduce resource overhead and improve overall BP model performance, including resource-efficient convolution, shortcut connection, and Huber loss.

6.2.1 Resource-efficient Convolution. The traditional design of the convolutional layer involves a large number of computations for tensor operations (i.e., high FLOPs). The underlying issue is that each layer output is intensively computed by performing channel-wise multiplications (i.e., using a single kernel to slide through all input channels) between the kernels and the input data (i.e., purified SCG or feature maps), especially when the input data has multiple channels and the filter size is large. Hence, it will result in high model inference latency when deployed on a smartphone. To reduce the number of operations, we utilize efficient depthwise separable convolution (DSConv) [15] in the proposed BP model. Technically, DSConv involves breaking down a standard convolution into two separate operations: depthwise convolution (DwConv) and pointwise convolution (PwConv), formulated as follows.

$$\begin{aligned} \text{DwConv } (k, i) &= \sum_{m=0}^{M-1} w_{(m,k)} * x_{(i+m,k)}, \\ \text{PwConv } (n, i) &= \sum_k^n w_{(i,k)} * x_{(i,k)}, \end{aligned} \quad (6)$$

where k and n denote the number of output channels of DwConv and PwConv, respectively. i denotes the channel index, and w denotes the weight of the kernel. Additionally, M is the size of the kernel, and x represents the input tensor. Different from the standard convolution, DwConv enables efficient multiplications that each input channel is convolved separately using its own kernel. This captures features independently for each input channel. While PwConv uniquely involves applying a 1x1 kernel to create linear combinations of the DwConv's output. This effectively combines features across different input channels, enabling the model to learn complex relationships



Fig. 7. Experimental setup.

between the channels. By both DwConv and PwConv operations, DSConv is mathematically represented as below.

$$\text{DSConv}(w_d, w_p, S) = \sum_k^N w_p(i, k) \cdot \left(\sum_{m=0}^{M-1} w_d(m, k) \cdot x(i+m, k) \right), \quad (7)$$

where w_d and w_p denote the kernel weights of DwConv and PwConv, respectively. D_S represents the width of feature maps, K and N denote the number of input and output channels of DSConv. Compared to the standard 1D convolution with computational complexity of $(M \cdot K \cdot N \cdot D_S)$, DSConv can theoretically achieve a much lower computational complexity due to the separate DwConv and PwConv. Specifically, the computational complexity of DwConv is $(M \cdot K \cdot D_S)$, while the computational complexity of PwConv is $(K \cdot N \cdot D_S)$. Combining these operations together, DSConv achieves a notable reduction in the computation of $(M \cdot K \cdot D_S + K \cdot N \cdot D_S)/M \cdot K \cdot N \cdot D_S = \frac{1}{N} + \frac{1}{M}$ [32], which uses 2 to 3 times less computation than the standard 1D convolution. Therefore, powered by DSConv and lightweight layer structure, our BP model achieves computationally resource efficiency, making the model fast to train and infer on smartphones.

6.2.2 Shortcut Connection. Since a small number of convolutional layers may be limited to extracting a comprehensive representation of features from the purified SCG, we essentially optimize our BP model with six DSConv layers based on the experiments. However, one of our observations shows that the model may still be subject to suboptimal performance due to the proposed number of layers. In traditional convolutional layers, the feature maps are forward passed through layer by layer and backward learned from computed gradients. As the number of layers increases, the gradients may be insufficiently learned (i.e., vanishing gradient problem) during training, hence it may yield model performance degradation.

To mitigate this problem, we propose to add shortcut connections (i.e., residual connections) [71] between the layers. Instead of complex layer-by-layer learning, the shortcut connection can create a direct mapping from one layer to the target layer, bypassing one or more intermediate layers (i.e., identity mapping [30]). Hence, the gradients can directly pass through the direct mapping to preserve gradient vanishing for sufficient weight learning. Mathematically, the shortcut connection is formulated as follows.

$$y = F(x, w_i) + x, \quad (8)$$

where x is the original input, and $F(x, w_i)$ is the learned direct mapping. Enabled by the shortcut connection, our BP model can effectively learn both shallow-level input features and high-dimensional features from deeper layers, resulting in enhanced model performance. In practice, we add a shortcut connection every 2 DSConv layers to group the layers as 3 residual blocks shown in Fig. 6.

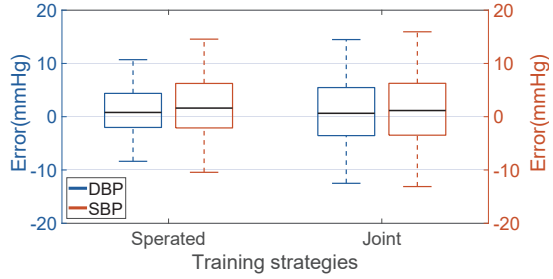


Fig. 8. Model performance with different training strategies.

6.2.3 Robust Training Schema. The performance of the learning loss function is critical to achieving high model robustness. Especially, the relationship between the purified SCG and BP may be easily impacted due to user and smartphone variations (i.e., subject-independent challenge) in SeismoBP. To enable a robust model training schema, we essentially apply Huber loss [48] in our BP model. Theoretically, it combines the advantages of the mean squared error (MSE) loss and the mean absolute error (MAE) loss, making it less sensitive to outliers compared to MSE while maintaining some of the smoothness properties of MAE, formulated as follows:

$$L(y, \hat{y}) = \begin{cases} \frac{1}{2}(y - \hat{y})^2, & \text{if } |y - \hat{y}| < 1, \\ |y - \hat{y}| - \frac{1}{2}, & \text{otherwise.} \end{cases} \quad (9)$$

We utilize the AdamW optimizer [29] during the training process and apply the early stopping mechanism [36] to optimize the model training. As a result, we propose a resource-efficient BP model to enable end-to-end BP prediction by taking the purified SCG with high model accuracy and robustness.

7 IMPLEMENTATION

Our prototype works as a smartphone app that uses its built-in accelerometer to capture SCG signals for BP measurement. We deploy the app on several commercial Android smartphones, i.e., Samsung Galaxy S5 with Android 6.0 OS, Samsung Galaxy S10 with Android 10.0 OS, and Xiaomi 13 with Android 13.0 OS, as shown in Fig. 7(a). We collect the accelerometer data from a smartphone and subsequently send it to a PC for processing. The accelerometer's sampling rate is set to 100 Hz which is sufficient to capture the frequency range of cardiac activity. To obtain the ground truth of BP, we use an FDA-approved cuff-based BP measurement device (Omron J751 [2]). Subjects are instructed to wear the cuff in a static setting, and the ground truth collected will be used as labels for training the BP estimation model. The accelerometer recordings are collected and sent to a LENOVO Y7000P PC through WiFi for processing using Python 3.11, i.e., denoising, enhancing data diversity, training the deep learning model, and estimating BP values.

The training of our BP model is done using an NVIDIA A100 GPU with 80GB of graphics memory. The specific parameter settings for the model include the following configurations within the Deep DsConv module: The kernel size of DWConv is set at 1×3 , and a stride size of 2 is employed, strategically reducing the feature size to incrementally enhance the model's performance. In the Deep DSConv module, we incorporate batch normalization and ReLU activation functions. A dropout rate of 0.2 is employed to alleviate potential overfitting. The model is trained using the Adam optimizer, employing an annealing learning rate that starts at 5e-3 and gradually decreases to 2.5e-4. The training proceeds for 100 epochs, incorporating an early stopping strategy.

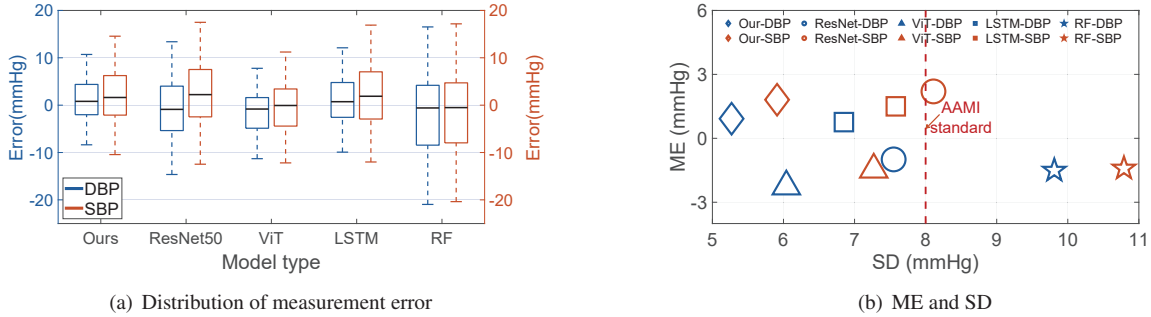


Fig. 9. Comparison of measurement error across different models.

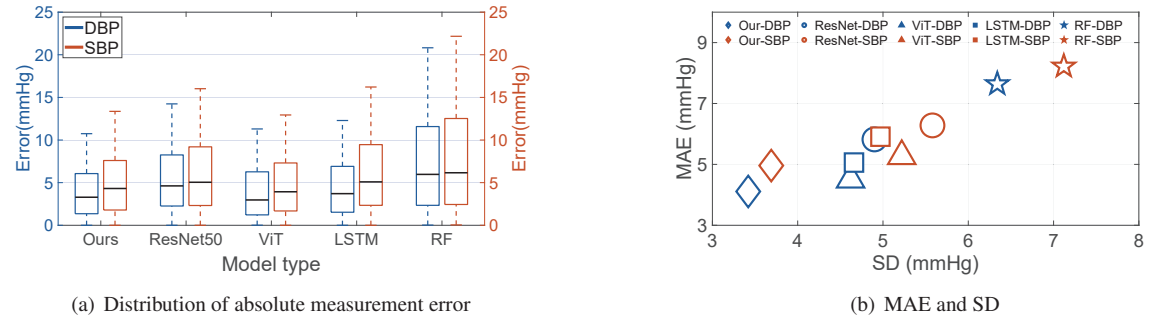


Fig. 10. Comparison of absolute measurement error across different models.

8 EVALUATIONS

8.1 Experimental Setup

We conduct all experiments in a typical room setting, keeping a comfortable room temperature between 20 and 25 °C. We recruit a total of 70 volunteers (28 females and 42 males), weighing between 45 and 90 Kg and aged from 22 to 83 years. The average age of the volunteers is 39 years, with an SD of 21. Among them, 35 are healthy, while the remaining 35 are diagnosed with high blood pressure, and some also have heart diseases such as arrhythmia, unstable angina (UA), and right bundle branch block (RBBB), with 5 patients for each heart disease. None of the volunteers have taken part in similar experiments before, and their heart rates range from 55 to 110 BPM, with an average of 76 BPM. We have obtained ethical approval from our institutional review board (IRB) prior to conducting any experiments. We begin each experiment with a 5-minute briefing session to introduce the experimental equipment and data collection methods. We ask volunteers to sit for 2 minutes in each data collection session to guarantee reliable results. During each session, they are instructed to wear a BP monitor cuff on their arm to measure BP, and simultaneously, they use a smartphone to collect SCG signals by pressing it perpendicularly on their chest, as illustrated in Fig. 7(b). From the 2 minutes of accelerometer data, a 10-second segment (comprising 1000 points at a 100 Hz sampling rate) is selected as one SCG sample, using the BP monitor readings as a reference. Considering the short-term stability of blood pressure, a mandatory 10-minute break is enforced between successive sessions to ensure variability in BP measurements. Therefore, each session has a duration of 12 minutes and includes just a single sample. For each volunteer, we collected a total of 10 samples

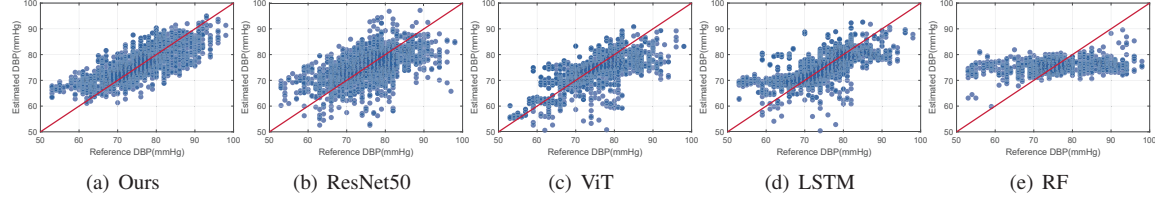


Fig. 11. Correlation of estimated DBP and reference across various models.

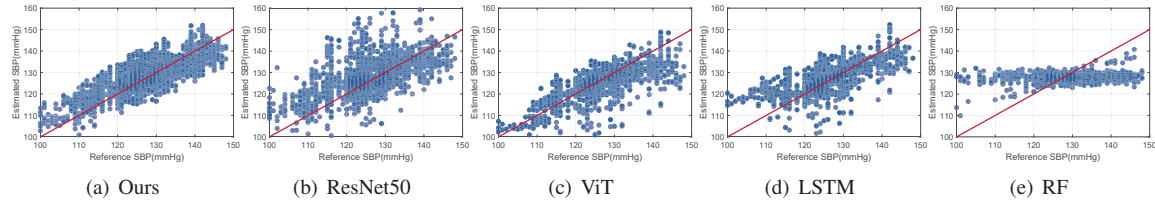


Fig. 12. Correlation of estimated SBP and reference across various models.

daily, spanning over a period of 2 hours. We conduct data collection on different days and times, accumulating a total of 100 samples for each subject. Unless stated otherwise, each subject takes part in all experiments, and we employ LOOCV to assess the system's performance using a user-independent data set. In detail, we divide the SCG data into n groups corresponding to n subjects, conducting testing through n iterations. During each iteration, we use the data from $n - 1$ subjects as the training samples, reserving the data from the remaining subject as the testing sample. In all experiments, we evaluate the system's performance using ME between the BP, including SBP and DBP, and the actual BP values, defined as $\mu = \sum_{n=1}^N \frac{b_n - \hat{b}_n}{N}$, where b_n denotes the estimation, \hat{b}_n represents the ground truth, N denotes the total number of testing samples. We also use SD, defined as $\delta = \sqrt{\sum_{n=1}^N \frac{(b_n - \hat{b}_n - \mu)^2}{N}}$, for this evaluation.

8.2 BP Model Performance

8.2.1 Training Strategies. We first evaluate whether different training strategies for BP regression may impact our model performance. We compare two training strategies—separated (i.e., separated models to estimate DBP and SBP, respectively) and joint (i.e., one model to estimate DBP and SBP simultaneously). We also use the leave-one-out cross-validation strategy detailed in Section 8.1. Since we apply the same input to estimate both DBP and SBP, the training process for each of them is balanced by default. As shown in Fig. 8, the results indicate that the performance of using separated models in both mean and standard error range aspects works notably better than using a joint model. For instance, by applying the separated models, the standard error range of SBP is reduced from 8.54 to 5.91, while the mean of SBP is also reduced from 2.17 to 1.81, and the standard error range of DBP significantly decreases from 6.75 to 5.27. Hence, we consistently use the separated training strategy in the next experiments.

8.2.2 Model Performance Comparison. We next conduct a comparative study between our model (Ours) and alternative popular deep learning models, including ResNet50, Vision Transformer (ViT), Long Short-Term Memory (LSTM), and Random Forest (RF) regression based on our dataset with detailed specifications shown in Section 8.1. We also apply the same training hyper-parameters (e.g., optimizer, learning rate, drop rate, epochs, and early stopping strategy) given in Section 7 to the baseline models as needed.

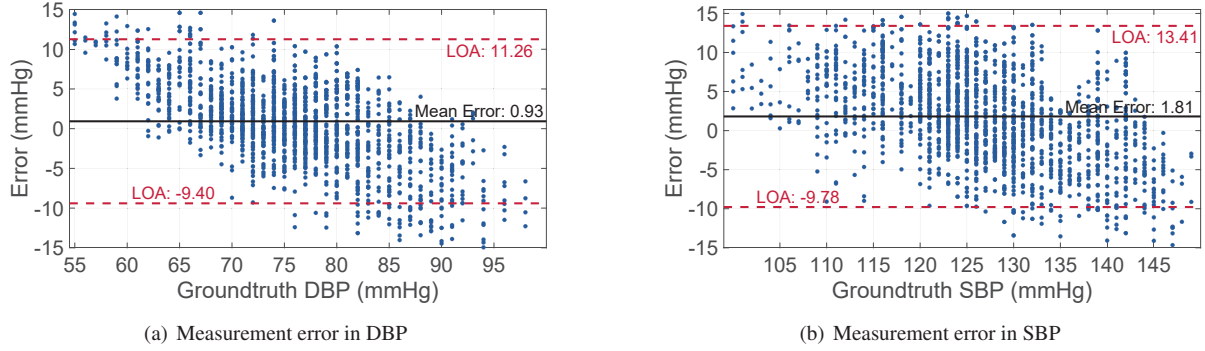


Fig. 13. Overall performance for the all users.

We also use LOOCV to assess the performance using different models, incorporating data from 70 users. The distribution of the measurement error is presented in Fig. 9(a). As illustrated in Fig. 9(b), for DBP, our model achieves an ME of 0.93 mmHg and SD of 5.27 mmHg. In comparison, the ME values of ResNet50, ViT, LSTM, and RF are -0.99 mmHg, -2.26 mmHg, 0.76 mmHg, and -1.51 mmHg, respectively, and their SD values are 7.55 mmHg, 6.05 mmHg, 6.85 mmHg, and 9.81 mmHg, respectively. For SBP, our model achieves an ME of 1.81 mmHg and SD of 5.91 mmHg, while the ME values of Resnet50, ViT, LSTM, and RF are 2.2 mmHg, -1.47 mmHg, 1.49 mmHg, and -1.41 mmHg, respectively, and their SD values are 8.11 mmHg, 7.27 mmHg, 7.59 mmHg, and 10.79 mmHg, respectively. It is evident that, for both DBP and SBP, our model achieves comparable performance to LSTM in terms of ME, but our SD is significantly lower than that of other models. This demonstrates our system's robust capacity for extracting features from multi-sample data.

To enhance the comparison of our model with others, we further analyze the distribution of absolute measurement errors (i.e., $b_n - \hat{b}_n$), as shown in Fig. 10(a), and calculated both the MAE (i.e., $\mu' = \sum_{n=1}^N \frac{|b_n - \hat{b}_n|}{N}$) and the SD of the absolute measurement errors (i.e., $\delta' = \sqrt{\sum_{n=1}^N \frac{(|b_n - \hat{b}_n| - \mu')^2}{N}}$), as depicted in Fig. 10(b). The results demonstrate that, for both SBP and DBP, our model significantly outperforms other models in terms of both MAE and SD, further highlighting the superior performance of our model.

Fig. 11 and Fig. 12 show the correlation between the measured DBP, SBP and reference BP, respectively. Here, the X-axis represents the reference, and the Y-axis represents the measurement results. Points on the red line indicate that the measured values are identical to the reference. Therefore, the closer the points are to the red line, the smaller the measurement error. We observe that compared to the other four models, points in our model are more closely clustered around the red line for both DBP and SBP, which indicates a closer correlation. The above results further demonstrate the effectiveness of our model in measuring BP. Specifically, we find that the predictions obtained from the RF model have a very low correlation with the reference points. Therefore, even if the results of ME fall within the AAMI standards, they are not meaningful for reference.

To provide a deeper insight into our system's performance, we present the Bland-Altman plots for both DBP and SBP, as illustrated in Fig. 13. In these plots, the black line represents ME, while the red line delineates the limits of agreement (LOA), defined as $ME \pm 1.96 \times SD$. Significantly, these errors fall within the standard error range established by the AAMI, which mandates that ME should not exceed 5 mmHg, and SD should not exceed 8 mmHg.

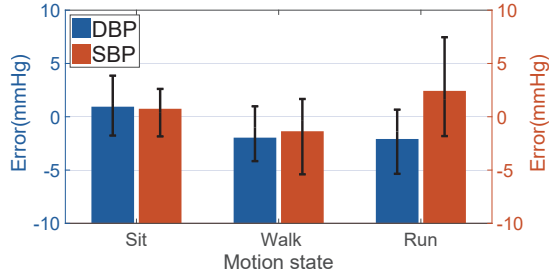


Fig. 14. Impact of different motion states.

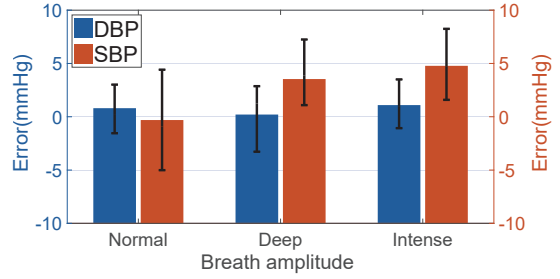


Fig. 15. Impact of different breath amplitudes.

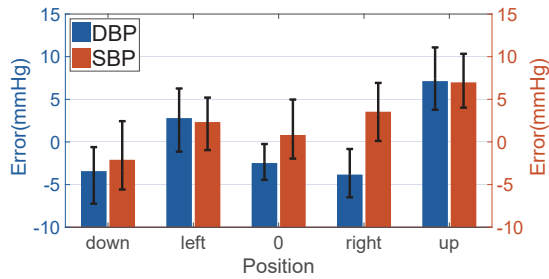


Fig. 16. Impact of different pressing positions.

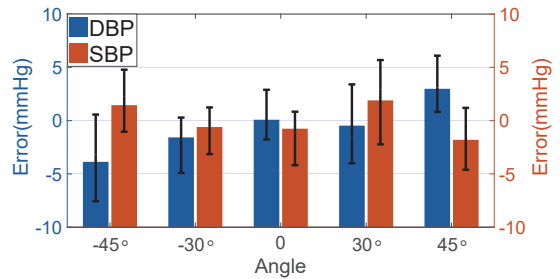


Fig. 17. Impact of different angles.

8.3 Evaluation of Impact Factors

In this section, we assess the robustness of our system in measuring BP under the influence of various factors. We use the original standardized data as training data and newly collected data under different conditions as the testing data. For example, when evaluating the system's performance in measuring variations due to different phone angles relative to the chest, we use data collected at different angles as the test data.

Impact of previous motion states: In this section, we concentrate on evaluating the system's performance in measuring blood pressure during the recovery period following various motion states. Specifically, we instruct each user to maintain three distinct motion states—sitting, walking, and running—and then collect data after a period of 2 minutes. All samples collected from these motion states are utilized as the training dataset to guarantee the diversity of the data. In detail, we collect 40 samples from each user in each of the motion states, amounting to a total of 120 samples per user, to ensure each motion state contributes equally to the training model. Fig. 14 shows that for DBP, the MEs after sitting, walking, and running states are 0.94 mmHg, -1.96 mmHg, and -2.08 mmHg, respectively. For SBP, the MEs after sitting, walking, and running states are 0.7 mmHg, -1.36 mmHg, and 2.43 mmHg, respectively. The changes in heart rate after walking do not affect the BP measurement performance, but the ME of SBP after running rises from 0.7 mmHg in a sitting state to 2.43 mmHg. This increase is mainly due to the active state of the body after running, such as intense hand tremors, which render the accelerometer signal more vulnerable to interference from bodily movement. Although running induces some error, the system still retains enough accuracy to meet the demands of daily monitoring. These outcomes verify that our system delivers robust blood pressure measurements during the recovery period after different motion states.

Impact of breath: We instruct volunteers to breathe at different amplitudes, including normal breath, deep breath, and intense breath. The data collected during normal breath served as the standard training sample. As depicted in

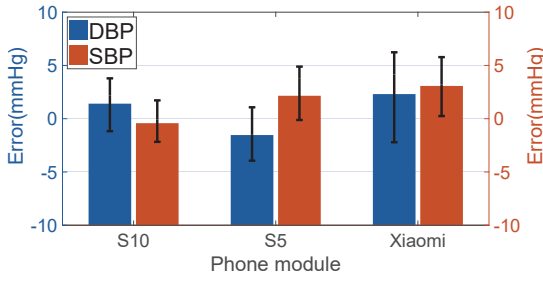


Fig. 18. Impact of different brands of phones.

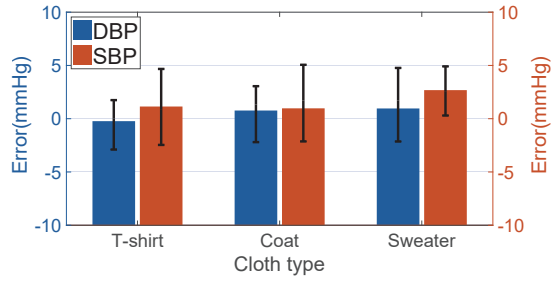


Fig. 19. Impact of different types of clothes.

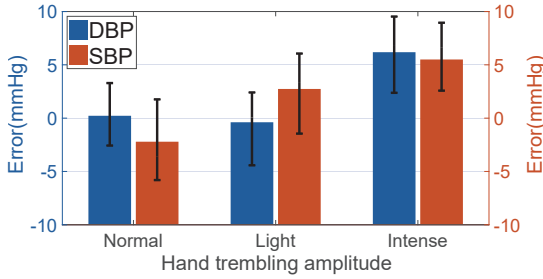


Fig. 20. Impact of different amplitudes of hand trembling.

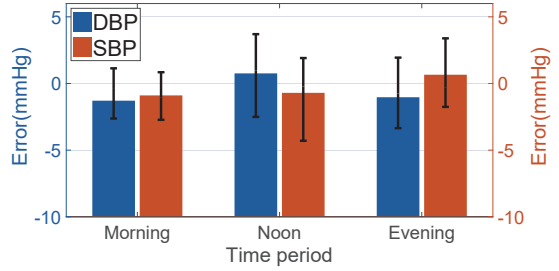


Fig. 21. Impact of different time periods.

Fig. 15, the average DBP errors for normal breath, deep breath, and intense breath are 0.8 mmHg, 0.21 mmHg, and 1.09 mmHg, respectively. The respective average errors for SBP are -0.31 mmHg, 3.54 mmHg, and 4.78 mmHg. With the increase in breath intensity, the error in BP also increases correspondingly, mainly because intense breath is usually accompanied by intense body movements. Although the error has increased, the mean error and standard deviation is still within the AAMI range. Therefore, our system can withstand the effects of different breath amplitudes. Additionally, by incorporating samples from intense breath into the training set, we can further improve BP measurement performance.

Impact of pressing position: To evaluate the impact of the pressing position on BP measurement, we initially designate the reference point's location on the subject's clothing, specifically at the center of the sternum. Then, we instruct the subject to press 5 cm left, right, up, and down from the reference point to measure the BP. Note that the samples collected from the reference point serve as training data, while those from other positions are used as testing data. As shown in Fig. 16, the error on the left side is close to the reference point, which is consistent with the fact that the heart is located on the left side of the chest. Nevertheless, the performance at the other three points diminishes to different extents, mainly because of a decrease in the SCG signals' amplitude. Overall, except for the position 5 cm above the reference point, the measurement performance near the reference point is sufficient to meet the needs of daily monitoring.

Impact of phone angle: To investigate the impact of phone angle on system performance, we positioned the phone at various angles against the chest, ranging from -45° to 45° . We defined the angle as 0° when the user held the phone vertically against the chest. When the phone is oriented upward, the angle is considered positive, and when facing downward, it is considered negative. As shown in Fig. 17, the system demonstrates high accuracy within a range of -30° to 30° , indicating that the heartbeat pattern is minimally affected by phone angle within this range.

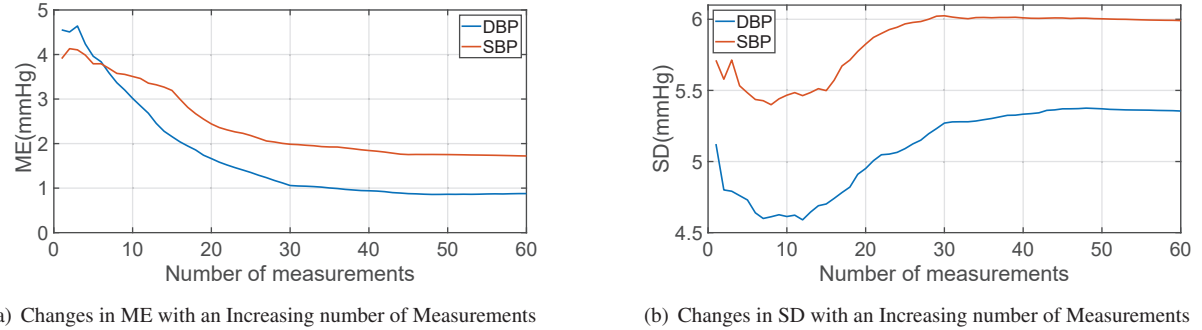


Fig. 22. Impact of various numbers of measurements.

However, as the angle continues to increase to -45° and 45° , the impact gradually increases, resulting in larger errors. This is mainly because the heartbeat activity is primarily concentrated in the front, allowing the phone to collect signals with higher SNR within a smaller angle range, while the SNR decreases in a larger range. Even with the worst average errors (i.e., DBP of -3.86 mmHg and a SBP of -1.8 mmHg), both the mean error and standard deviation remain within the AAMI standard range, thus meeting the criteria for daily monitoring.

Impact of phone type: We deploy our system on three smartphones, namely Samsung Galaxy S10, Samsung Galaxy S5, and Xiaomi 13, to investigate the capability of various phone modules in estimating BP. Note that the training data is exclusively collected from the Samsung Galaxy S10. In this part, we collect new data from three different types of smartphones, which are then utilized as testing data for comparison. As shown in Fig. 18, the average errors in DBP for the three phones are 1.41 mmHg, -1.53 mmHg, and 2.31 mmHg, respectively, and the average errors in SBP are -0.42 mmHg, 2.15 mmHg, and 3.08 mmHg, respectively. Although Xiaomi 13 had more noise compared to Samsung Galaxy S10 and Samsung Galaxy S5, its BP prediction performance is on par with the other two modules. This is mainly attributed to our triple-stage noise reduction scheme, which effectively eliminated system noise. Overall, the experimental results demonstrate the effective deployment capability of our system across different types of smartphones.

Impact of cloth type : To simulate clothing for different seasons, we have volunteers wear T-shirts, coats, and sweaters respectively while collecting acceleration data. We use the data collected while wearing T-shirts as the standard training data. Fig. 19 shows that the average interval errors of the three garments are nearly identical, with the maximum average errors for DBP and SBP being 0.96 and 2.68 , respectively. Although an increase in clothing thickness may cause a slight rise in measurement error, our system still possesses the ability to accurately predict BP.

Impact of hand trembling: To assess our system's resilience to artificial noise, we instruct subjects to shake their mobile phones at three distinct intensities—normal, light, and intense—during the course of the experiment. The data collected under normal conditions is utilized as the standard training set, while the data corresponding to the two other amplitudes are only employed as the test set. As illustrated in Fig. 20, the measurement error of BP grows with an increase in amplitude of hand trembling. When an intensive hand trembling occurs, the system's measurement error exceeds the AAMI standard range. However, during light hand trembling, the system still demonstrates excellent BP prediction performance, mainly attributable to our triple-stage noise reduction scheme, which effectively filters out the impact of movement artifacts.

Impact of time period: To investigate the system's stability throughout the day, we collect BP data from users at various times. Fig. 21 demonstrates that our system exhibits high stability at various times throughout the day. This

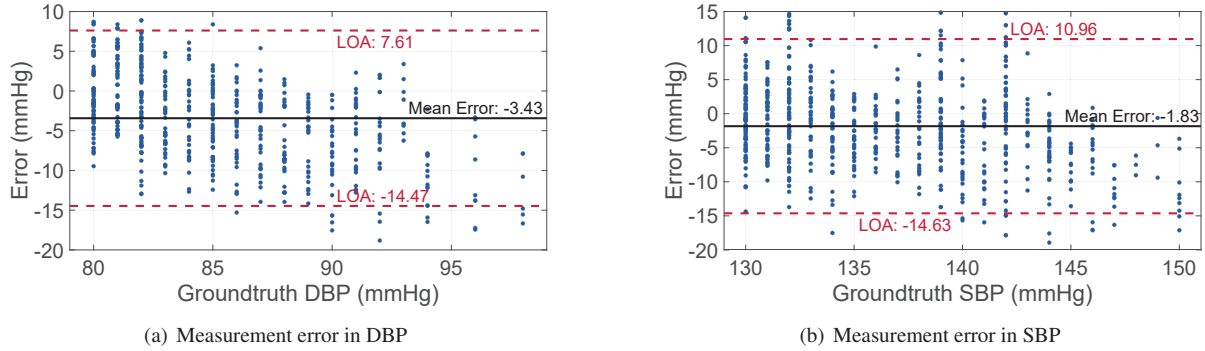


Fig. 23. Performance for the patient with high blood pressure.

stability can primarily be attributed to the fact that the heartbeat pattern remains consistent, despite fluctuations in BP over the course of the day. Consequently, this indicates that our system possesses strong robustness across different time periods.

Impact of the number of measurements: To explore the impact of number of measurements on system performance, we collect a range of samples from each user, varying from 1 to 60, and then analyze their measurement errors. As shown in Fig. 22, with the increase in the number of measurements, the average ME continuously decreases while the SD first decreases and then increases. After reaching 30 measurements, both tend to converge. The changes in ME and SD are reasonable: at the beginning, when the number of measurements is small, the data randomness is relatively high. As the number of measurements reaches a certain level, the data tends to stabilize. These results indicate that continuous measurements of 30 times or more can result in the stabilization of our system's performance. Note that our initial measurement requires the collection of 10 seconds of SCG data, yet the system's response time is measured in milliseconds. Additionally, the interval between measurements is kept to just 1 second to ensure timely data refreshment. Consequently, the total time required for 30 measurements is approximately 40 seconds, which is acceptable for daily monitoring applications.

8.4 Ablation Study

To investigate the effectiveness of technologies in the signal preprocessing part, we conduct ablation study on four key steps in the noise reduction: ICEEMDAN, RLS-based filter, soft-thresholding, and data enhancement. Specifically, we conducted a reprocessing of the original data. This involved removing the corresponding techniques to create new training and testing datasets for additional four deep learning models, respectively. Subsequently, we re-evaluated the data from 70 users (100 samples per user) using LOOCV, as detailed in Section 8.1. As shown in Fig. 24(a), for DBP, our system's ME is 0.93 mmHg, whereas the MEs after removing ICEEMDAN, RLS-based filter, soft-thresholding, and data enhancement are -1.22 mmHg, -2.15 mmHg, -1.05 mmHg, and -2.53 mmHg, respectively. Correspondingly, the SD increases from 5.27 mmHg to 7.1 mmHg, 9.01 mmHg, 6.53 mmHg, and 7.44 mmHg, respectively. Additionally, as shown in Fig. 24(b), for SBP, our system's ME is 1.81 mmHg, while the MEs after removing ICEEMDAN, RLS-based filter, soft-thresholding, and data enhancement are 2.98 mmHg, 3.8 mmHg, 2.06 mmHg, and 4.4 mmHg, respectively. The SD also changes from 5.92 mmHg to 7.5 mmHg, 8.93 mmHg, 8.41 mmHg, and 8.35 mmHg, respectively. These results adequately demonstrate that preprocessing related technologies can significantly improve the performance of BP measurement. Particularly, the RLS-based filter and data enhancement have a notably evident impact on performance improvement. This is mainly attributed to the substantial reduction of movement artifact by the RLS-based filter and the effective increase in data diversity by data enhancement.

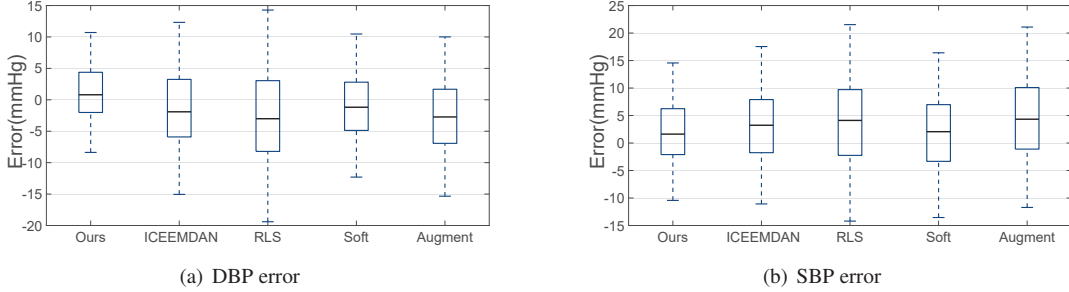


Fig. 24. Ablation study on noise reduction and data augmentation.

8.5 Case Study on Diseases

To further evaluate the measurement performance of our system, we recruit 35 hypertensive patients, of whom 15 have different heart diseases, including arrhythmia, unstable angina, and right bundle branch block, with 5 patients for each condition. The purpose of this subsection is to explore whether our system can effectively measure BP in patients with relevant cardiovascular diseases. We adopt a leave-one-out cross-validation strategy, as detailed in Section 8.1. For example, to evaluate the performance of the system in arrhythmia, we conducted 5 tests, using the data of one patient as the test set and the data of the remaining 69 subjects as the training set in each iteration. Finally, we collate all the results to evaluate the overall performance of the system.

Hypertension: In this study, we investigate whether the system can accurately measure blood pressure for 35 hypertensive patients. According to the latest hypertension standards set by the American Heart Association [3], individuals with $DBP \geq 80$ and $SBP \geq 130$ are diagnosed with hypertension. To elucidate the system's measurement proficiency, we specifically assess the BP readings of hypertensive patients upon meeting these criteria. It should be noted that hypertensive patients regularly take medication to control their condition, so they may not necessarily experience high blood pressure during the experiment. As a result, our data collection shows that SBP samples are typically less than 150 and DBP samples are less than 100. When BP is too high, patients may experience symptoms such as dizziness and palpitations, which can exacerbate their discomfort during data collection. We present the Bland-Altman plots for SBP and DBP, as shown in Fig. 23. In the figure, the black line denotes ME, while the red line signifies LOA. The results indicate that the ME and SD for DBP are -3.43 mmHg and 5.63 mmHg, respectively, while those for SBP are -1.83 mmHg and 6.52 mmHg. Compared to the overall performance in Section 8.2.2, this result is slightly lower, mainly due to fewer hypertension samples, resulting in a lack of sample diversity (only accounting for 28.8% of the total samples). We believe that increasing hypertension samples can further improve the results. Overall, the current measurement performance conforms to the AAMI standards for mean error and standard deviation.

Arrhythmia: Arrhythmia refers to an abnormality in heart rhythm, primarily categorized into tachycardia, bradycardia, and sinus arrhythmia. Such abnormalities typically lead to variations in the intervals between heartbeats. As our system relies on the waveform characteristics of heartbeats to estimate BP, it's crucial to further investigate its measurement accuracy for hypertensive patients with arrhythmias. We assess five hypertensive patients with arrhythmias: one with tachycardia, one with bradycardia, and three with sinus arrhythmias. As illustrated in Fig. 25, the ME for DBP and SBP are -0.46 mmHg and 0.25 mmHg, respectively, with corresponding SD of 5.81 mmHg and 6.05 mmHg. These findings suggest that our system can accurately measure the BP of such patients.

Unstable angina: Unstable angina is a type of coronary cardiac disease, primarily manifested as chest pain or discomfort caused by transient myocardial ischemia. Hypertension is closely related to it and may lead to the occurrence of unstable angina. Compared to a healthy individual, the patient's heartbeat pattern exhibits significant

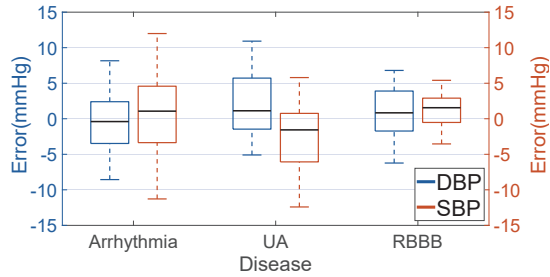


Fig. 25. Performance on different cardiac diseases.

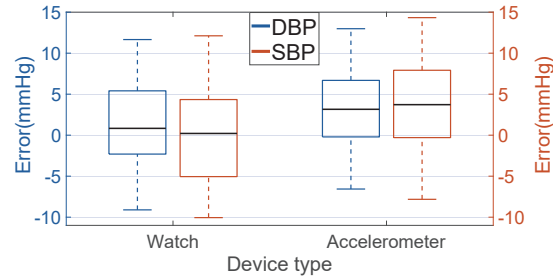


Fig. 26. Performance on commercial devices.

variations. For example, the Electrocardiograph (ECG) of patients with this condition typically exhibits noticeable waveform changes, such as T-wave inversion. As depicted in Fig. 25, from the analysis of data collected from five patients diagnosed with both unstable angina and hypertension, we observe that the ME and SD for DBP are 1.47 mmHg and 5.11 mmHg, respectively. For SBP, these values are -2.48 mmHg and 5.21 mmHg, respectively. These results confirm that our system can accurately measure the BP of such patients.

Right bundle branch block: RBBB represents a disruption in the heart’s right bundle branch conduction system, hindering the efficient transmission of electrical signals to the ventricles. Under this condition, the patient’s cardiac rhythm exhibits specific changes, such as the T wave being opposite in direction to the QRS wave. Chronic hypertension may cause left ventricular hypertrophy and cardiac remodeling. These changes can alter the heart’s electrophysiological properties, leading many hypertensive patients to develop RBBB. Based on this, we investigate whether our system could accurately measure BP in such patients. We analyze the data from 5 patients diagnosed with both RBBB and hypertension. As depicted in Fig. 25, the ME and SD values for DBP stand at 0.38 mmHg and 4.44 mmHg, respectively. For SBP, the values are 1.24 mmHg and 3.02 mmHg. Our results validate that our system offers a high degree of accuracy in monitoring BP for patients afflicted with unstable angina and hypertension.

8.6 Case Study on Commercial Devices

To validate the versatility of our model across different platforms, we conduct an experiment involving 10 new subjects. We position a Samsung Watch5 and a commercial accelerometer sensor, WT901WIFI [4], on the chests of the subjects to capture SCG signals. Given the disparate sampling rates of the watch, accelerometer sensor, and smartphone accelerometer, we employ spline interpolation to standardize their sampling rates. Subsequently, we assess the BP measurement accuracy for the 10 subjects using the BP model, which is trained on Samsung Galaxy 10 data. It is important to note that the model has not been exposed to the data from any of the subjects prior to this, and this data is exclusively used for testing purposes. As depicted in Fig. 26, the system demonstrates high measurement accuracy for both the watch and the accelerometer sensor, confirming the viability of our system for cross-platform BP measurement.

9 SYSTEM LATENCY AND POWER CONSUMPTION

System latency: Our system achieves low latency, rendering it suitable for real-time blood pressure monitoring. We deploy the system on a Samsung Galaxy S10 smartphone, outfitted with a 2.9 GHz octa-core Qualcomm SM8150 Snapdragon CPU. Our implementation employs a dual-thread architecture, comprising a display thread and a blood pressure measurement thread. For processing SCG signals, our system utilizes a buffer that accommodates 640 data samples (equivalent to 6.4 s), updating it every 4 s to ensure the application delivers 10 measurement results within a window of 40 s. Across 100 measurements, our system consistently requires an average of 18.9 ms to implement

the triple-stage noise reduction technique on buffer data. The time needed for blood pressure measurement via a deep learning model amounts to 45.68 ms. Consequently, the overall latency of our system stands at a mere $18.9 + 45.68 = 64.58$ ms (substantially under 4 s), a duration wholly suitable for real-time blood pressure monitoring.

Power consumption: Our system demonstrates efficient energy consumption, averaging 182.2 ± 8.6 mW on commercially available smartphones. We employ PowerTutor [67] to assess the power utilization of our system on Samsung Galaxy S10. The average power consumption is evaluated over a two-hour period, segmented into six 20-minute sessions. During each session, the user executes 20 blood pressure measurement operations. Excluding the power consumed by the LCD display, the observed average CPU power consumption stands at 182.2 ± 8.6 mW.

10 DISCUSSION AND FUTURE WORK

Currently, our system faces three issues that need to be addressed:

Large-scale movements: Although our system's three-step denoising scheme can mitigate the impact of general movements, including deep breathing and hand tremors, it remains ineffective at accurately reconstructing heartbeat waveforms to estimate blood pressure in the presence of large-scale movements, such as running or walking. In future work, we will resort to more advanced noise reduction schemes to enhance the system's robustness.

Unseen heart diseases: Our blood pressure system can accurately predict cross-subject blood pressure for diseases present in the training set, but it performs poorly with previously unseen disease types. This is primarily because different heart diseases correspond to different heartbeat patterns. In the future, we need to collect data from patients with a variety of heart diseases to broaden the system's applicability.

Phone types: So far, our system has only been validated on three Android phone types, which is insufficient. In the future, we need to validate our system on a wider range of phone types, and additionally, we need to develop a blood pressure measurement system for iOS to ensure the system's applicability across most brands.

11 CONCLUSION

This paper presents a novel sensing system that captures SCG signals using smartphone's built-in accelerometer, facilitating accurate BP measurement. Our system outperforms previous mobile phone-based BP measurement systems by offering high SNR, ease of use, and power efficiency. To reconstruct high-quality heartbeat waveforms from noisy SCG signals, we propose a triple-stage noise reduction scheme that incorporates ICEEMDAN, RLS adaptive filtering, and soft-thresholding. In addition, we propose a data augmentation technique involving normalization and *temporal-sliding* to augment the diversity within the training sample set. To ensure battery efficiency on smartphones, we introduce a resource-efficient deep learning model which incorporates resource-efficient convolution, shortcut connections, and Huber loss. We successfully deploy our system on three smartphone models and evaluate its performance through extensive experiments with 70 volunteers, including 35 healthy and 35 hypertensive individuals, in a user-independent scenario. Experimental results confirm that our system is robust and accurate for daily BP measurement.

ACKNOWLEDGMENTS

This research is supported by National Natural Science Foundation of China (Grant No. 62102006). This work is also in part supported by The Natural Science Foundation of the Jiangsu Higher Education Institutions of China (Grant No. 1020231697). The corresponding author is Haipeng Dai.

REFERENCES

- [1] 2017. Global Health Observatory data: Raised blood pressure. <https://apps.who.int/gho/data/node.main.A875STANDARD?lang=en>.
- [2] 2023. Omron blood pressure monitor. <https://omronhealthcare.com/blood-pressure/>.

- [3] 2023. Understanding Blood Pressure Readings. <https://www.heart.org/en/health-topics/high-blood-pressure/understanding-blood-pressure-readings>.
- [4] 2023. WitMotion WT901WIFI. <https://www.wit-motion.com/iot-gyroscope/witmotion-wt901wifi-wireless.html>.
- [5] PM Agante and JP Marques De Sá. 1999. ECG noise filtering using wavelets with soft-thresholding methods. In *Computers in Cardiology 1999. Vol. 26 (Cat. No. 99CH37004)*. IEEE, 535–538.
- [6] Sanghyun Baek, Jiyong Jang, Sung-Hwan Cho, Jong Min Choi, and Sungroh Yoon. 2020. Blood pressure prediction by a smartphone sensor using fully convolutional networks. In *Proceedings of IEEE EMBC*.
- [7] Fabian Beutel, Chris Van Hoof, Xavier Rottenberg, Koen Reesink, and Evelien Hermeling. 2021. Pulse arrival time segmentation into cardiac and vascular intervals—implications for pulse wave velocity and blood pressure estimation. *IEEE Transactions on Biomedical Engineering* 68, 9 (2021), 2810–2820.
- [8] Dilpreet Buxi, Jean-Michel Redouté, and Mehmet Rasit Yuce. 2016. Blood pressure estimation using pulse transit time from bioimpedance and continuous wave radar. *IEEE Transactions on Biomedical Engineering* 64, 4 (2016), 917–927.
- [9] Yetong Cao, Huijie Chen, Fan Li, and Yu Wang. 2021. Crisp-BP: Continuous wrist PPG-based blood pressure measurement. In *Proceedings of ACM MobiCom*.
- [10] Andrew M Carek, Jordan Conant, Anirudh Joshi, Hyolim Kang, and Omer T Inan. 2017. SeismoWatch: wearable cuffless blood pressure monitoring using pulse transit time. *Proceedings of the ACM on interactive, mobile, wearable and ubiquitous technologies* 1, 3 (2017), 1–16.
- [11] Anand Chandrasekhar, Chang-Sei Kim, Mohammed Naji, Keerthana Natarajan, Jin-Oh Hahn, and Ramakrishna Mukkamala. 2018. Smartphone-based blood pressure monitoring via the oscillometric finger-pressing method. *Science translational medicine* 10, 431 (2018), eaap8674.
- [12] Anand Chandrasekhar, Mohammad Yavarimanesh, Keerthana Natarajan, Jin-Oh Hahn, and Ramakrishna Mukkamala. 2020. PPG sensor contact pressure should be taken into account for cuff-less blood pressure measurement. *IEEE Transactions on Biomedical Engineering* 67, 11 (2020), 3134–3140.
- [13] Eric Chang, Chung-Kuan Cheng, Anushka Gupta, Po-Han Hsu, Po-Ya Hsu, Hsin-Li Liu, Amanda Moffitt, Alissa Ren, Irene Tsaur, and Samuel Wang. 2019. Cuff-less blood pressure monitoring with a 3-axis accelerometer. In *Proceedings of IEEE EMBC*.
- [14] Yanjiao Chen, Baolin Zheng, Zihan Zhang, Qian Wang, Chao Shen, and Qian Zhang. 2020. Deep Learning on Mobile and Embedded Devices: State-of-the-Art, Challenges, and Future Directions. *ACM Comput. Surv.* (2020).
- [15] Francois Fleuret. 2017. Xception: Deep Learning With Depthwise Separable Convolutions. In *Proceedings of IEEE/CVF CVPR*.
- [16] John Cioffi and Thomas Kailath. 1984. Fast, recursive-least-squares transversal filters for adaptive filtering. *IEEE Transactions on Acoustics, Speech, and Signal Processing* 32, 2 (1984), 304–337.
- [17] Israel Cohen, Yiteng Huang, Jingdong Chen, Jacob Benesty, Jacob Benesty, Jingdong Chen, Yiteng Huang, and Israel Cohen. 2009. Pearson correlation coefficient. *Noise reduction in speech processing* (2009), 1–4.
- [18] Marcelo A Colominas, Gastón Schlotthauer, and María E Torres. 2014. Improved complete ensemble EMD: A suitable tool for biomedical signal processing. *Biomedical Signal Processing and Control* 14 (2014), 19–29.
- [19] Richard S Crow, Peter Hannan, David Jacobs, Lowell Hedquist, and David M Salerno. 1994. Relationship between seismocardiogram and echocardiogram for events in the cardiac cycle. *American Journal of Noninvasive Cardiology* 8 (1994), 39–46.
- [20] Jean Degott, Arlene Ghajarzadeh-Wurzner, Gregory Hofmann, Martin Proenca, Guillaume Bonnier, Alia Lemkadem, Mathieu Lemay, Urvan Christen, Jean-François Knebel, Virginie Durnat, et al. 2021. Smartphone based blood pressure measurement: accuracy of the OptiBP mobile application according to the AAMI/ESH/ISO universal validation protocol. *Blood Pressure Monitoring* 26, 6 (2021), 441.
- [21] M Di Rienzo, E Vaini, P Castiglioni, G Merati, P Meriggi, G Parati, A Faini, and F Rizzo. 2013. Wearable seismocardiography: Towards a beat-by-beat assessment of cardiac mechanics in ambulant subjects. *Autonomic Neuroscience* 178, 1-2 (2013), 50–59.
- [22] David L Donoho. 1995. De-noising by soft-thresholding. *IEEE Transactions on Information Theory* 41, 3 (1995), 613–627.
- [23] Lorenz Frey, Carlo Menon, and Mohamed Elgendi. 2022. Blood pressure measurement using only a smartphone. *npj Digital Medicine* 5, 1 (2022), 86.
- [24] Hidekatsu Fukuta and William C Little. 2008. The cardiac cycle and the physiologic basis of left ventricular contraction, ejection, relaxation, and filling. *Heart failure clinics* 4, 1 (2008), 1–11.
- [25] Aman Gaurav, Maram Maheedhar, Vijay N Tiwari, and Rangavittal Narayanan. 2016. Cuff-less PPG based continuous blood pressure monitoring—A smartphone based approach. In *Proceedings of IEEE EMBC*.
- [26] LA Geddes, MH Voelz, CF Babbs, JD Bourland, and WA Tacker. 1981. Pulse transit time as an indicator of arterial blood pressure. *psychophysiology* 18, 1 (1981), 71–74.
- [27] Shrimanti Ghosh, Ankur Banerjee, Nilanjan Ray, Peter W Wood, Pierre Boulanger, and Raj Padwal. 2016. Continuous blood pressure prediction from pulse transit time using ECG and PPG signals. In *Proceedings of IEEE HI-POCT*.
- [28] JS Gravenstein, David A Paulus, Jeffrey Feldman, and Gayle McLaughlin. 1985. Tissue hypoxia distal to a Penaz finger blood pressure cuff. *Journal of clinical monitoring* 1 (1985), 120–125.
- [29] Lei Guan. 2023. Weight Prediction Boosts the Convergence of AdamW. In *Advances in Knowledge Discovery and Data Mining*.

- [30] Kaiming He, Xiangyu Zhang, Shaoqing Ren, and Jian Sun. 2016. Identity Mappings in Deep Residual Networks. In *Computer Vision – ECCV 2016*.
- [31] Christopher E Heil and David F Walnut. 1989. Continuous and discrete wavelet transforms. *SIAM review* 31, 4 (1989), 628–666.
- [32] Andrew Howard, Menglong Zhu, Bo Chen, Dmitry Kalenichenko, Weijun Wang, Tobias Weyand, Marco Andreetto, and Hartwig Adam. 2017. MobileNets: Efficient Convolutional Neural Networks for Mobile Vision Applications. (2017).
- [33] Norden E Huang, Zheng Shen, Steven R Long, Manli C Wu, Hsing H Shih, Quanan Zheng, Nai-Chyuan Yen, Chi Chao Tung, and Henry H Liu. 1998. The empirical mode decomposition and the Hilbert spectrum for nonlinear and non-stationary time series analysis. In *Proceedings of the Royal Society of London A: Mathematical, Physical and Engineering Sciences*.
- [34] Toan Huu Huynh, Roozbeh Jafari, and Wan-Young Chung. 2018. A robust bioimpedance structure for smartwatch-based blood pressure monitoring. *Sensors* 18, 7 (2018).
- [35] Mohammad Shamim Imtiaz, Rajeeva Shrestha, Talwinder Dhillon, Kazi Ata Yousuf, Bilal Saeed, Anh Dinh, and Khan Wahid. 2013. Correlation between seismocardiogram and systolic blood pressure. In *Proceedings of IEEE CCECE*.
- [36] Ziwei Ji, Justin Li, and Matus Telgarsky. 2021. Early-stopped neural networks are consistent. In *NeurIPS '21*.
- [37] Jessi E Johnson, Oliver Shay, Chris Kim, and Catherine Liao. 2019. Wearable millimeter-wave device for contactless measurement of arterial pulses. *IEEE transactions on biomedical circuits and systems* 13, 6 (2019), 1525–1534.
- [38] Kjel A Johnson, Deborah J Partsch, Patrick Gleason, and Kelly Makay. 1999. Comparison of two home blood pressure monitors with a mercury sphygmomanometer in an ambulatory population. *Pharmacotherapy: The Journal of Human Pharmacology and Drug Therapy* 19, 3 (1999), 333–339.
- [39] Jeena Joy, Salice Peter, and Neetha John. 2013. Denoising using soft thresholding. *International Journal of Advanced Research in Electrical, Electronics and Instrumentation Engineering* 2, 3 (2013), 1027–1032.
- [40] Alair Dias Junior, Srinivasan Murali, Francisco Rincon, and David Atienza. 2015. Estimation of blood pressure and pulse transit time using your smartphone. In *Proceedings of IEEE DSD*.
- [41] Ryota Kawasaki and Akihiro Kajiwara. 2021. Continuous blood pressure monitoring with MMW radar sensor. *IEICE Communications Express* 10, 12 (2021), 997–1002.
- [42] Ryota Kawasaki and Akihiro Kajiwara. 2022. Continuous blood pressure estimation using millimeter wave radar. In *lproc IEEE RWS*.
- [43] Insoo Kim and Yusuf A Bhagat. 2016. Towards development of a mobile RF Doppler sensor for continuous heart rate variability and blood pressure monitoring. In *Proceedings of IEEE EMBC*.
- [44] Federica Landreani, Alba Martín-Yebra, Claudia Casellato, Carlo Frigo, Esteban Pavan, Pierre-François Migeotte, and Enrico G Caiani. 2016. Beat-to-beat heart rate detection by smartphone's accelerometers: validation with ECG. In *Proceedings of IEEE EMBC*.
- [45] Catherine Liao, Oliver Shay, Elizabeth Gomes, and Nikhil Bikhchandani. 2021. Noninvasive continuous blood pressure measurement with wearable millimeter wave device. In *Proceedings of IEEE BSN*.
- [46] MM Llabre, GH Ironson, SB Spitzer, MD Gellman, DJ Weidler, and N Schneiderman. 1988. How many blood pressure measurements are enough?: An application of generalizability theory to the study of blood pressure reliability. *Psychophysiology* 25, 1 (1988), 97–106.
- [47] Kenta Matsumura, Peter Rolfe, Sogo Toda, and Takehiro Yamakoshi. 2018. Cuffless blood pressure estimation using only a smartphone. *Scientific reports* 8, 1 (2018), 7298.
- [48] Gregory P. Meyer. 2021. An Alternative Probabilistic Interpretation of the Huber Loss. In *Proceedings of IEEE/CVF CVPR*.
- [49] Reham Mohamed and Moustafa Youssef. 2017. Heartsense: Ubiquitous accurate multi-modal fusion-based heart rate estimation using smartphones. *Proceedings of the ACM on Interactive, Mobile, Wearable and Ubiquitous Technologies* 1, 3 (2017), 1–18.
- [50] Osval Antonio Montesinos López, Abelardo Montesinos López, and Jose Crossa. 2022. *Overfitting, Model Tuning, and Evaluation of Prediction Performance*.
- [51] Guy P Nason and Bernard W Silverman. 1995. The stationary wavelet transform and some statistical applications. In *Wavelets and statistics*. Springer, 281–299.
- [52] Takayoshi Ohkubo, Kei Asayama, Masahiro Kikuya, Hirohito Metoki, Haruhisa Hoshi, Junichiro Hashimoto, Kazuhito Totsune, Hiroshi Satoh, and Yutaka Imai. 2004. How many times should blood pressure be measured at home for better prediction of stroke risk? Ten-year follow-up results from the Ohasama study. *Journal of hypertension* 22, 6 (2004), 1099–1104.
- [53] Mikko Paukkunen, Petteri Parkkila, Tero Hurnanen, Mikko Päkkälä, Tero Koivisto, Tuomo Nieminen, Raimo Kettunen, and Raimo Sepponen. 2015. Beat-by-beat quantification of cardiac cycle events detected from three-dimensional precordial acceleration signals. *IEEE journal of biomedical and health informatics* 20, 2 (2015), 435–439.
- [54] Thomas Pickering. 2001. The case for a hybrid sphygmomanometer. *Blood Pressure Monitoring* 6, 4 (2001), 177–179.
- [55] Carla Sala, Erika Santin, Marta Rescaldani, Cesare Cuspidi, and Fabio Magrini. 2005. What is the accuracy of clinic blood pressure measurement? *American journal of hypertension* 18, 2 (2005), 244–248.
- [56] Alma Secerbegovic, Jacob Bergsland, Per Steinar Halvorsen, Nermin Suljanovic, Aljo Mujcic, and Ilangko Balasingham. 2016. Blood pressure estimation using video plethysmography. In *Proceedings of IEEE ISBI*.
- [57] JingYao Shi and KangYoon Lee. 2022. Systolic blood pressure measurement algorithm with mmWave radar sensor. *KSII Transactions on Internet and Information Systems (TIIS)* 16, 4 (2022), 1209–1223.

- [58] Zhenguo Shi, Tao Gu, Yu Zhang, and Xi Zhang. 2022. mmBP: Contact-Free Millimetre-Wave Radar Based Approach to Blood Pressure Measurement. In *Proceedings of ACM SenSys*.
- [59] Sungtae Shin, Azin Sadat Mousavi, Sophia Lyle, Elisabeth Jang, Peyman Yousefian, Ramakrishna Mukkamala, Dae-Geun Jang, Ui Kun Kwon, Youn Ho Kim, and Jin-Oh Hahn. 2021. Posture-dependent variability in wrist ballistocardiogram-photoplethysmogram pulse transit time: implication to cuff-less blood pressure tracking. *IEEE Transactions on Biomedical Engineering* 69, 1 (2021), 347–355.
- [60] Szymon Sieciński and Paweł Kostka. 2018. Determining heart rate beat-to-beat from smartphone seismocardiograms: Preliminary studies. In *Innovations in Biomedical Engineering*. Springer, 133–140.
- [61] J Talts, R Raamat, K Jagomägi, and J Kivastik. 2011. An influence of multiple affecting factors on characteristic ratios of oscillometric blood pressure measurement. In *Proceedings of Springer NBC*.
- [62] Simi Susan Thomas, Viswam Nathan, Chengzhi Zong, Ebunoluwa Akinbola, Antoine Lourdes Praveen Aroul, Lijoy Philipose, Karthikeyan Soundarapandian, Xiangrong Shi, and Roozbeh Jafari. 2014. BioWatch—A wrist watch based signal acquisition system for physiological signals including blood pressure. In *Proceedings of IEEE EMBC*.
- [63] María E Torres, Marcelo A Colominas, Gastón Schlotthauer, and Patrick Flandrin. 2011. A complete ensemble empirical mode decomposition with adaptive noise. In *Proceedings of IEEE ICASSP*.
- [64] Edward Jay Wang, Junyi Zhu, Mohit Jain, Tien-Jui Lee, Elliot Saba, Lama Nachman, and Shwetak N Patel. 2018. Seismo: Blood pressure monitoring using built-in smartphone accelerometer and camera. In *Proceedings of ACM CHI*.
- [65] Yinan Xuan, Colin Barry, Jessica De Souza, Jessica H Wen, Nick Antipa, Alison A Moore, and Edward J Wang. 2023. Ultra-low-cost mechanical smartphone attachment for no-calibration blood pressure measurement. *Scientific Reports* 13, 1 (2023), 8105.
- [66] Yukino Yamaoka, Jiang Liu, and Shirgeru Shimamoto. 2019. Detections of pulse and blood pressure employing 5G millimeter wave signal. In *Proceedings of IEEE CCNC*.
- [67] Z Yang. 2012. Powertutor-a power monitor for android-based mobile platforms. *EECS, University of Michigan, retrieved September 2 (2012)*, 19.
- [68] Youngzoon Yoon, Jung H Cho, and Gilwon Yoon. 2009. Non-constrained blood pressure monitoring using ECG and PPG for personal healthcare. *Journal of medical systems* 33 (2009), 261–266.
- [69] Peyman Yousefian, Sungtae Shin, Azin Sadat Mousavi, Ali Tivay, Chang-Sei Kim, Ramakrishna Mukkamala, Dae-Geun Jang, Byung Hoon Ko, Jongwook Lee, Ui-Kun Kwon, et al. 2020. Pulse transit time-pulse wave analysis fusion based on wearable wrist ballistocardiogram for cuff-less blood pressure trend tracking. *IEEE Access* 8 (2020), 138077–138087.
- [70] Kaja Fjørtoft Ystgaard, Luigi Atzori, David Palma, Poul Einar Heegaard, Lene Elisabeth Bertheussen, Magnus Rom Jensen, and Katrien De Moor. 2023. Review of the theory, principles, and design requirements of human-centric Internet of Things (IoT). *Journal of Ambient Intelligence and Humanized Computing* (2023).
- [71] Ke Zhang, Miao Sun, Tony X. Han, Xingfang Yuan, Liru Guo, and Tao Liu. 2018. Residual Networks of Residual Networks: Multilevel Residual Networks. *IEEE Transactions on Circuits and Systems for Video Technology* (2018).
- [72] Yu Zhang, Tao Gu, and Xi Zhang. 2020. MDLdroidLite: a Release-and-Inhibit Control Approach to Resource-Efficient Deep Neural Networks on Mobile Devices. In *Proceedings of ACM SenSys*.
- [73] Heng Zhao, Xu Gu, Hong Hong, Yusheng Li, Xiaohua Zhu, and Changzhi Li. 2018. Non-contact beat-to-beat blood pressure measurement using continuous wave Doppler radar. In *Proceedings of IEEE/MTT-S IMS*.